AFRL-AFOSR-VA-TR-2016-0036

Spider Silk: From Protein-rich Gland Fluids to Diverse Biopolymer Fibers

Gregory Holland
ARIZONA STATE UNIVERSITY
660 S MILL AVE STE 312
TEMPE, AZ 85281

01/06/2016
Final Report

Air Force Research Laboratory
AF Office Of Scientific Research (AFOSR)/RTB2

Arlington, Virginia 22203
Air Force Materiel Command

REPORT DOCUMENTATION PAGE

Form Approved
OMB No. 0704-0188

1. REPORT DATE *(DD-MM-YYYY)*	2. REPORT TYPE	3. DATES COVERED *(From - To)*
06-01-2016	Final Performance	01-12-2013 to 30-11-2015

4. TITLE AND SUBTITLE
Spider Silk: From Protein-rich Gland Fluids to Diverse Biopolymer Fibers

5a. CONTRACT NUMBER

5b. GRANT NUMBER
FA9550-14-1-0014

5c. PROGRAM ELEMENT NUMBER
61102F

6. AUTHOR(S)
Gregory Holland

5d. PROJECT NUMBER

5e. TASK NUMBER

5f. WORK UNIT NUMBER

7. PERFORMING ORGANIZATION NAME(S) AND ADDRESS(ES)
ARIZONA STATE UNIVERSITY
660 S MILL AVE STE 312
TEMPE, AZ 85281 US

8. PERFORMING ORGANIZATION REPORT NUMBER

9. SPONSORING/MONITORING AGENCY NAME(S) AND ADDRESS(ES)
AF Office of Scientific Research
875 N. Randolph St. Room 3112
Arlington, VA 22203

10. SPONSOR/MONITOR'S ACRONYM(S)
AFRL/AFOSR RTB2

11. SPONSOR/MONITOR'S REPORT NUMBER(S)

12. DISTRIBUTION/AVAILABILITY STATEMENT
A DISTRIBUTION UNLIMITED: PB Public Release

13. SUPPLEMENTARY NOTES

14. ABSTRACT

The primary objective of this research is to elucidate the interactions, mechanisms and biochemistry of the spider silk producing process at the
molecular level. Our primary focus is to characterize the protein-rich fluid in the various spider silk producing glands. We have been using a battery
of magnetic resonance methods including solution and solid-state nuclear magnetic resonance (NMR) and micro imaging (MRI) in combination
with wide angle and small angle X-ray diffraction (WAXD and SAXD) techniques at Argonne National Laboratory (ANL) to probe silk protein
structure and dynamics prior to and following fiber formation. We have established a number of methods for isotopically (2H/13C/15N) enriching
the silk proteins during the course of our AFOSR funding that have allowed us to investigate the structure, dynamics, and organization of spider
silk protein within the silk gland and in the final spun fiber with a range of magnetic resonance methods. We successfully developed magnetic
resonance imaging (MRI) techniques with localized spectroscopy to probe the silk glands of spiders and map protein structure through out the silk
gland.

15. SUBJECT TERMS
Silk, nmr

16. SECURITY CLASSIFICATION OF:			17. LIMITATION OF ABSTRACT	18. NUMBER OF PAGES	19a. NAME OF RESPONSIBLE PERSON
a. REPORT	b. ABSTRACT	c. THIS PAGE			Gregory Holland
Unclassified	Unclassified	Unclassified	UU		19b. TELEPHONE NUMBER *(Include area code)* 619-594-1596

Standard Form 298 (Rev. 8/98)
Prescribed by ANSI Std. Z39.18

1. Cover Sheet:

To: technicalreports@afosr.af.mil
Subject: Final Performance Report to Dr. Hugh DeLong

Contract/Grant Title: Spider's Silk: From Protein-Rich Gland Fluids to Diverse Biopolymer Fibers

PIs: Gregory P. Holland and Jeffery L. Yarger

Institution: Department of Chemistry and Biochemistry, Arizona State University, Tempe AZ 85287-1604

Contract/Grant #: FA9550-14-1-0014

Reporting Period: 1 December 2013 to 30 November 2015

2. Objectives (taken directly from the original proposal):

Spider's produce up to seven different types of silk that range in mechanical properties from tougher than Kevlar to the extensibility of rubber and have the potential for numerous military applications ranging from high performance textiles and vehicle tires to biological scaffolding and biomedical materials. However, because of the inability to domesticate spiders and the small amount of material produced, we must first be able to manufacture the fiber in large quantities, and this requires that spider silk be produced with recombinant protein methods in the laboratory. With the advent of DNA sequencing of numerous spider silks and the expression of these sequences in several different biological hosts, scientists have moved closer to this end goal. To date, however, numerous synthetic spider silks have been made with either partial or full primary amino acid sequences, but none match the mechanical properties of native spider silks. This is primarily due to differences in the spinning process (engineering) and the resultant differences in secondary, tertiary and quaternary folded structure of the silk proteins that comprise the fiber. Hence, the ability to reproduce spider silk fibers in the laboratory (synthetic silk), relies on a molecular understanding of how spiders produce insoluble silk fibers with a diverse range of mechanical properties from an aqueous protein-rich spinning dope in the gland. The objective of the proposed research is to elucidate the interactions, mechanisms and chemistries of the spider silk producing process at the molecular level for a range of spider silks. Our primary focus is to characterize the protein-rich fluid in the various silk producing glands. Although we have begun to understand the molecular features of the protein-rich fluid in the major ampullate gland and the resulting structure and dynamics of dragline silk fibers, still little to no molecular level detail is available regarding the other spinning dopes and silks. In addition to interrogating the protein structure in the gland, it is important to understand the molecular dynamics of the proteins and the secondary and tertiary structure of other types of spider silks (e.g. minor ampullate, tubuliform and aciniform silk). The proposed work aims to move beyond the spinning process of dragline silk and move into studying the dopes spiders use to spin egg cases (tubuliform and aciniform) and wrap prey (aciniform). We plan to utilize a combination of nuclear magnetic resonance (NMR) methods in conjunction with x-ray diffraction (XRD) in collaboration with Argonne National Laboratories (ANL) to achieve this goal. A list of specific aims that Profs. Holland and Yarger hope to achieve in the proposed research is given below:

- Conduct high-resolution NMR spectroscopy of various (major, minor, tubuliform, aciniform) isotopically enriched glands dissected from different species of spider to characterize the molecular structure and dynamics of the spider silk proteins in the gland. This will involve completely assigning the ^{1}H, ^{13}C and ^{15}N NMR spectra of the proteins in the gland with three-dimensional (3D) multi-nuclear liquid-state NMR methods to determine if the proteins in the gland exhibit secondary, tertiary and/or quaternary structure.
- We will elucidate the molecular dynamics of the proteins in the spinning dopes with $^{1}H/^{15}N$ two-dimensional (2D) relaxation (T_1 and T_2), nuclear Overhauser enhancement (NOE) measurements and pulsed field gradient (PFG) techniques for determining protein diffusion coefficients.
- Determine with NMR spectroscopy if changing the pH, temperature, or salt (Na^+, K^+) of the gland fluid promotes aggregation and/or protein folding into β-sheet,

helical and turn-like structures and/or impacts the silk proteins' molecular dynamics in the dope.

- Utilize modern solid-state NMR techniques (e.g. multi-dimensional $^{1}H/^{13}C/^{15}N$ triple resonance experiments with dipolar recoupling) to characterize fibers and gland fluids that have been processed in various ways including dehydration, methanol treatment, and variability in salt concentration and exposed to mechanical stress. Establish the relevant processing conditions for converting the isotropic gland fluid to a fibrous material rich in crystalline β-sheets and other secondary structural elements that are present in native spider silks.
- Perform x-ray diffraction (XRD) measurements on gland fluids that have been processed under the above stated conditions to detect the presence of β-sheet or other crystalline structures. Utilize XRD methods to determine the domain size and dimensions of the crystalline component and compare to native spider silks.
- Develop magnetic resonance imaging (MRI) as an in situ technique to interrogate the spider silk producing process. Micro-image spider glands and ducts on in tact spiders, conduct localized NMR spectroscopy, diffusion weighted imaging and pH sensitive chemical exchange saturation transfer (CEST) imaging on the contents of various glands and ducts.

The primary intellectual merit of the proposed project is focused on uncovering the fundamental molecular mechanisms for converting spider gland fluids to high-performance fibers using a suite of magnetic resonance (NMR and MRI) spectroscopic and XRD methods. It is our hope that this will lead to broader impacts in the synthetic silk and biopolymer community as well as help advance these materials for DoD applications.

3.1 Status of Effort (Year 1):

The primary objective of this research is to elucidate the interactions, mechanisms and biochemistry of the spider silk producing process at the molecular level. Our primary focus is to characterize the protein-rich fluid in the various spider silk producing glands. We have been using a battery of magnetic resonance methods including solution and solid-state nuclear magnetic resonance (NMR) and micro imaging (MRI) in combination with wide angle and small angle X-ray diffraction (WAXD and SAXD) techniques at Argonne National Laboratory (ANL) to probe silk protein structure and dynamics prior to and following fiber formation. We have established a number of methods for isotopically ($^{2}H/^{13}C/^{15}N$) enriching the silk proteins during the course of our AFOSR funding that have allowed us to investigate the structure, dynamics, and organization of spider silk protein within the silk gland and in the final spun fiber. The latter primarily involves incorporating a combination of ^{2}H and ^{13}C isotope labels as spin probes for interrogating backbone and sidechain molecular dynamics. One particular highlight was using this technique to elucidate dynamic changes in the GPGXX β-turn regions of major ampullate spidroin 2 (MaSp2) when *Argiope aurantia* spider silks are wet and supercontracted (see *Chem. Commun.* **2014**, *50*, 4856). We also began investigating the structure of aquatic silks spun by Caddisfly (see *Biomacromolecules* **2014**, *15*, 1269) and nanofiber silks produced by Webspinners (see *RSC Advances* **2014**, *4*, 41301). Lastly, we continued to develop magnetic resonance imaging (MRI) techniques with localized spectroscopy to probe the silk glands of spiders.

3.1 Status of Effort (Year 2):

In year 2 we continued using $^{2}H/^{13}C$ isotopes to investigate the dyanmics of spider silk proteins in dry and wet fibers by probing the Ala-rich regions in *Nephila clavipes* dragline (*Biomacromolecules* **2015**, *16*, 852). In addition, we successfully developed an *in vitro* solid-state NMR approach to monitor the kinetics of spider silk assembly from the gland fluid to β-sheet rich fibers (see *Biomacromolecules* **2015**, *16*, 2072). This will be a powerful approach for monitoring the impact of various biochemical-processing conditions on spider silk formation moving forward with this project. In addition to NMR methods, we have been developing WAXD and SAXD diffraction methods in collaboration with ANL to probe hierarchical nanoscale organization of β-sheet nanocrystallites in different types of spider silks from various species. Lastly, we continue to develop MRI as an *in vivo* tool for interrogating silk protein structure and dynamics within the different silk glands and have been moving in a new direction where we are imaging and conducting localized ^{1}H NMR spectroscopy on silkworms where the internal spinning system is considerably larger compared to spiders.

4.1 Accomplishments/New Findings (Year 1):

Our research team has made considerable headway in understanding the dynamics of spider silk proteins in the silk fibers when dry and water wetted (supercontracted) during the first year of the funding period. In one notable example, we enriched *Argiope aurantia* dragline silk with $^{2}H/^{13}C/^{15}N$-Proline and probed the proline dynamics by analyzing ^{2}H magic angle spinning (MAS) sideband patterns (SSBs) extracted from ^{2}H-^{13}C heteronuclear correlation (HETCOR) NMR spectra and comparing the results with simulations. This allowed us to directly probe both the backbone and sidechain dynamics of the major ampullate spidroin 2 (MaSp2) GPGXX β-turn region when the silk was dry and supercontracted with water. An example of ^{2}H-^{13}C HETCOR spectra together with ^{2}H MAS simulations for the dry spider silk is presented in Figure 1. Proline side-chain molecular motion can be described by each CD_2 undergoing a two-site reorientation. To interpret this motion for each site,

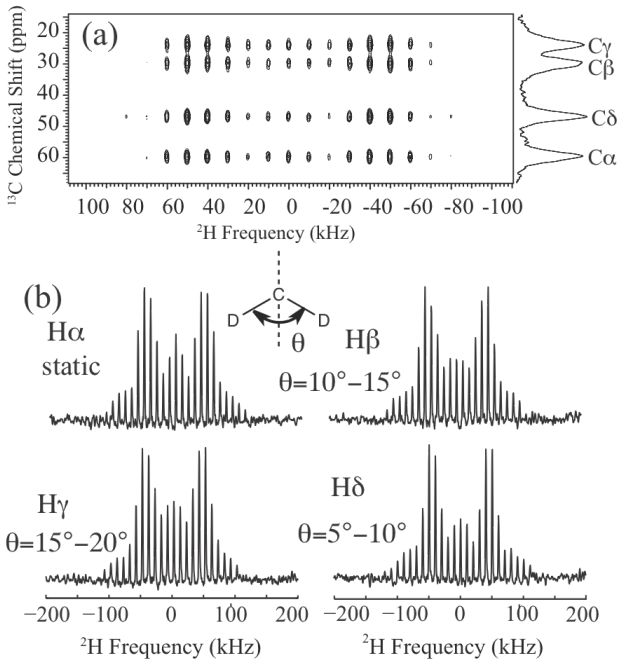

Figure. 1 (a) ^{2}H-^{13}C HETCOR MAS NMR spectrum for U-[$^{2}H_7$,$^{13}C_5$,^{15}N]-Pro labelled *A. aurantia* dragline silk. (b) Pro ^{2}H line shapes extracted from the 2D spectrum and the dynamics proposed for each site. Pro side-chain dynamics is described by each CD_2 undergoing fast reorientation between two sites separated by an angle θ. The angles are extracted from comparing experimental ^{2}H line shapes with simulations.

^{2}H line shape simulations were conducted and compared with the experimental data. The results illustrated that each deuterium on the side-chain undergoes fast two-site reorientation at an angle of 10°-15°, 15°-20° and 5°-10° for Pro ^{2}Hβ, ^{2}Hγ and ^{2}Hδ, respectively (see Figure 1b). The corresponding reorientation rates are greater than 10^8 s^{-1}. Pro residues in spider dragline silk (GPGXX motif) undergo much smaller reorientation angles when compared to crystalline proline illustrating the rigidity of this domain when the silk is dry. A static MAS pattern was observed for Pro ^{2}Hα, illustrating that the Pro backbone environment ($<10^2$ s^{-1}) in dry spider dragline silk is completely rigid.

Considerable dynamic changes were detected with the ^{2}H MAS NMR approach was applied to dragline silk that was wet and supercontracted. These results are preesented in Figure 2. These experiments illustrate that the large Pro ^{2}H spinning sideband (SSBs) pattern observed in dry silk are reduced to a central peak accompanied by one set of weak SSBs when the silk is wet and supercontracted. Significant signal loss was observed for the supercontracted silk in fully relaxed ^{2}H solid-echo and one-pulse MAS NMR spectra compared to the dry silk. For the wet supercontracted silk, the central peak cannot be fit to one peak possessing a Lorentzian, Gaussian or combined lineshape. Instead, fits of ^{2}H 1D data indicate the existence of two components, a broad (~3.8 kHz FWHM) and narrow peak (~400 Hz FWHM). The broad component is indicative of microsecond dynamics for a Pro deuterium population. This dynamical process could be the motion of the Pro local backbone along the fiber axis as no additional bond on the side-chain is available besides the fast two-site reorientations of the CD_2 as discussed above. This backbone motion can be described by a simple model were the entire Pro residue undergoes a three site reorientation along an external axis with a rate of 3×10^6 s^{-1} (Figure 2). The axis is considered the long axis of the local protein backbone. The observed ^{2}H signal loss is due to the short T_2 of the broad component, a consequence of molecular dynamics in the microsecond regime. In contrast, the narrow component obtained from

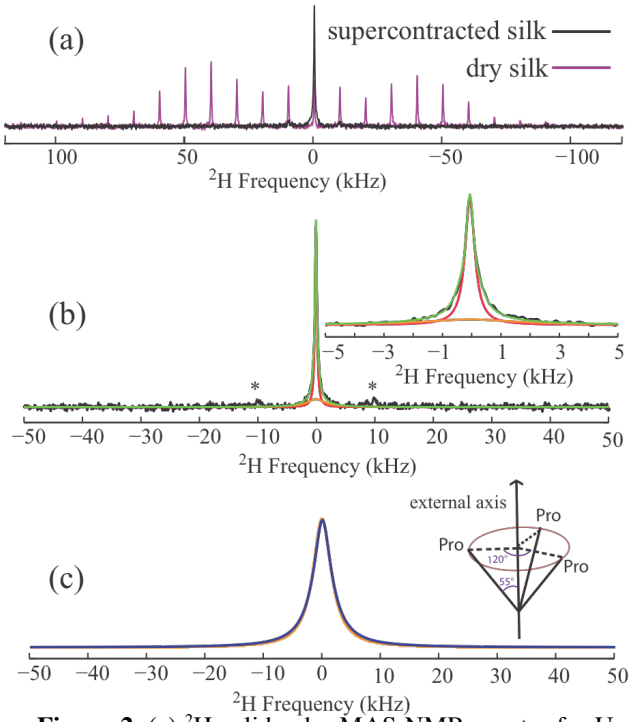

Figure 2. (a) ^{2}H solid-echo MAS NMR spectra for U-[$^2H_7$,$^{13}C_5$,^{15}N]-Pro labelled *A. aurantia* dragline silk in the dry and supercontracted (wet) state. (b) ^{2}H solid-echo MAS spectrum of supercontracted (wet) silk (black, same one as show in (a) and its fit (green). The central peak region is expanded and shown on the upper right. A broad (orange) and narrow (red) component was used for the fit. The asterisks indicate the spinning sidebands. (c) Experimental (orange) and simulated ^{2}H line shape (blue). A model of the entire Pro residue undergoing a three-site reorientation along an external axis is shown.

the fit corresponds to a proline population that becomes extremely mobile (near isotropic) due to strong interactions with water. This mobile proline population accounts for 30-35% of the signal thus, 65-70% of the proline undergoes microsecond backbone motions when the silk is wet and supercontracted.

These results allowed us to come up with both a structural and dynamical model for what happens to the GPGXX β-turn regions unique to MaSp2 since, proline is only found in this motif in spider dragline silk. From the primary protein sequence, the GPGXX motifs typically repeat 3-5 times and are sandwiched between the poly-Ala and poly-(GA) domains that form rigid nanocrystalline β-sheets. Hence, it is reasonable to propose that the GPGXX motifs near β-sheet regions (within two repeats) exhibit microsecond motions when the silk is supercontracted, because the dynamics are likely restricted by the flanking rigid β-sheet domains that remain rigid. In contrast, hydrated GPGXX motifs located further away from the β-sheet regions (>2 repeat units) are less constrained by the crystalline regions and undergo much faster, near isotropic motion. Combining the silk protein primary sequence with the molecular motion revealed by ^{2}H NMR, a model was proposed for Pro side-chain and the local protein backbone in dry and wet, supercontracted silk (see Figure 3). For more info on this work see *Chem. Commun.* **2014**, *50*, 4856.

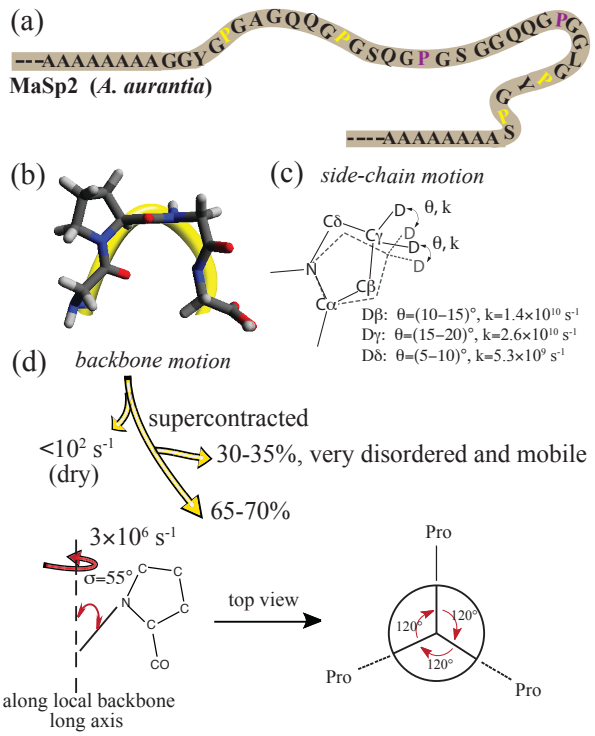

Figure. 3 Proposed protein backbone and side-chain dynamics for Pro-containing motifs in *A. aurantia* dragline silk fibre. (a) Primary amino acid sequence of MaSp2 repetitive motifs. (b) Schematic representation of type II β-turn structure for Pro-rich motif. The shown structural element is Gly-Pro-Gly-Ala. (c) Pro side-chain dynamics in the native, dry silk fibre where the Pro side-chain CD_2 undergo fast reorientation between two sites separated by an angle θ. Pro side-chains become much more mobile when the silk is wet, supercontracted (not shown). (d) Backbone dynamics for wet, supercontracted silk, 65-70% of Pro-containing regions (highlighted in yellow in a) exhibit 3×10^6 s^{-1} backbone motion. The mobility of the remaining 30-35% Pro-rich regions (highlighted in purple in a) is near isotropic.

Durring the year one funding period, we expanded into new types of animal silks including aquatic fibers spun by caddisflies. Caddisfly larvae use adhesive, aquatic silk fibers to stitch together debris into elaborate underwater assemblies. Although caddisflies are closely related to Lepidopteran insects, including the *Bombyx Mori* silkworm, their silk fibers do not contain poly(Ala) or poly(Gly-Ala) motifs that form the β-sheet rich structures in silkworm and spider silks. Instead,

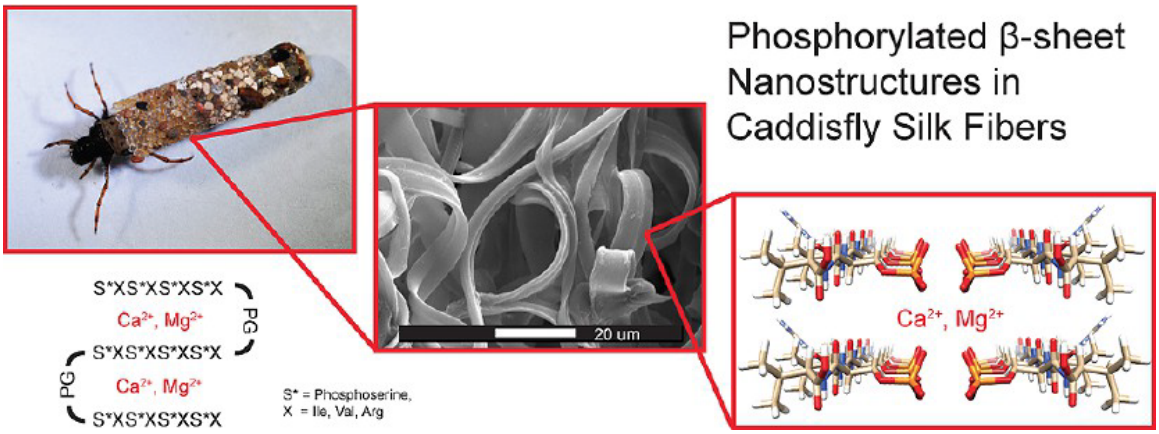

Figure 4. Image of a caddisfly with gems stitched together with the fly's adhesive silk. A SEM micrograph showing the flat, ribbon-like morphology of caddisfly silk and a model of the divalent cation stabilized phosphorylated serine-rich β-sheet nanostructures. The model was developed based on a combination of ^{13}C and ^{31}P solid-state NMR and XRD data collected by our research team for caddisfly silk (see *Biomacromolecules* **2013**, *14*, 1140).

caddisfly silks contain phosphorylated $(Ser\text{-}X)_4$ repeat units that are thought to be charge stabilized via divalent cations such as Ca^{2+} (see Figure 4 for image of caddisfly, caddisfly silk and molecular model of the phosphorylated Ser-rich β-sheet nanocrysalline structure).

We used a combination of solid-state NMR, XRD and electron microscopy techniques to probe the structural importance of divalent cation stabilized phosphorylated Ser-rich complexes within caddisfly silks. Scanning electron microscopy (SEM) experiments conducted on caddisfly silks before and after ethylenediaminetetraaacetic acid (EDTA) chelation treatment are presented in Figure 5. The native caddisfly silk prior to EDTA treatment is a fusion of two fibrils into a flat, ribbon-like fiber. Each fiber is comprised of smaller (~120 nm) nanofibrils (see Figure 5 A, B). When the silk is treated with EDTA the fiber morphology is completely destroyed. Instead of 5-10 μm wide ribbons, the silk becomes warped and inconsistent with exposed, disorganized nanofibers (see Figure 5 C, D) .

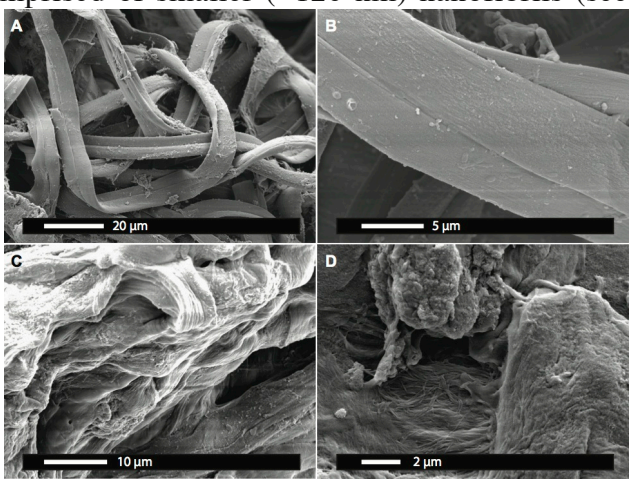

Figure 5. Scanning electron microscopy (SEM) images of native caddisfly silk (A and B) and silk treated with EDTA solution (C and D). The fibers are destroyed when Ca^{2+} is removed through EDTA chelation. The images were collected on gold-coated samples using an XL30 Environmental SEM-FEG.

WAXD data on native caddisfly silk show that the silk contains a significant crystalline fraction with a repetitive orthorhobic unit cell aligned along the fiber axis with dimensions of 5.9 Å x 23.2 Å x 17.3 Å. These nanocrystalline domains depend on the presence of multivalent cations that can be extracted from the silk by using a sufficent chelation agent like EDTA.

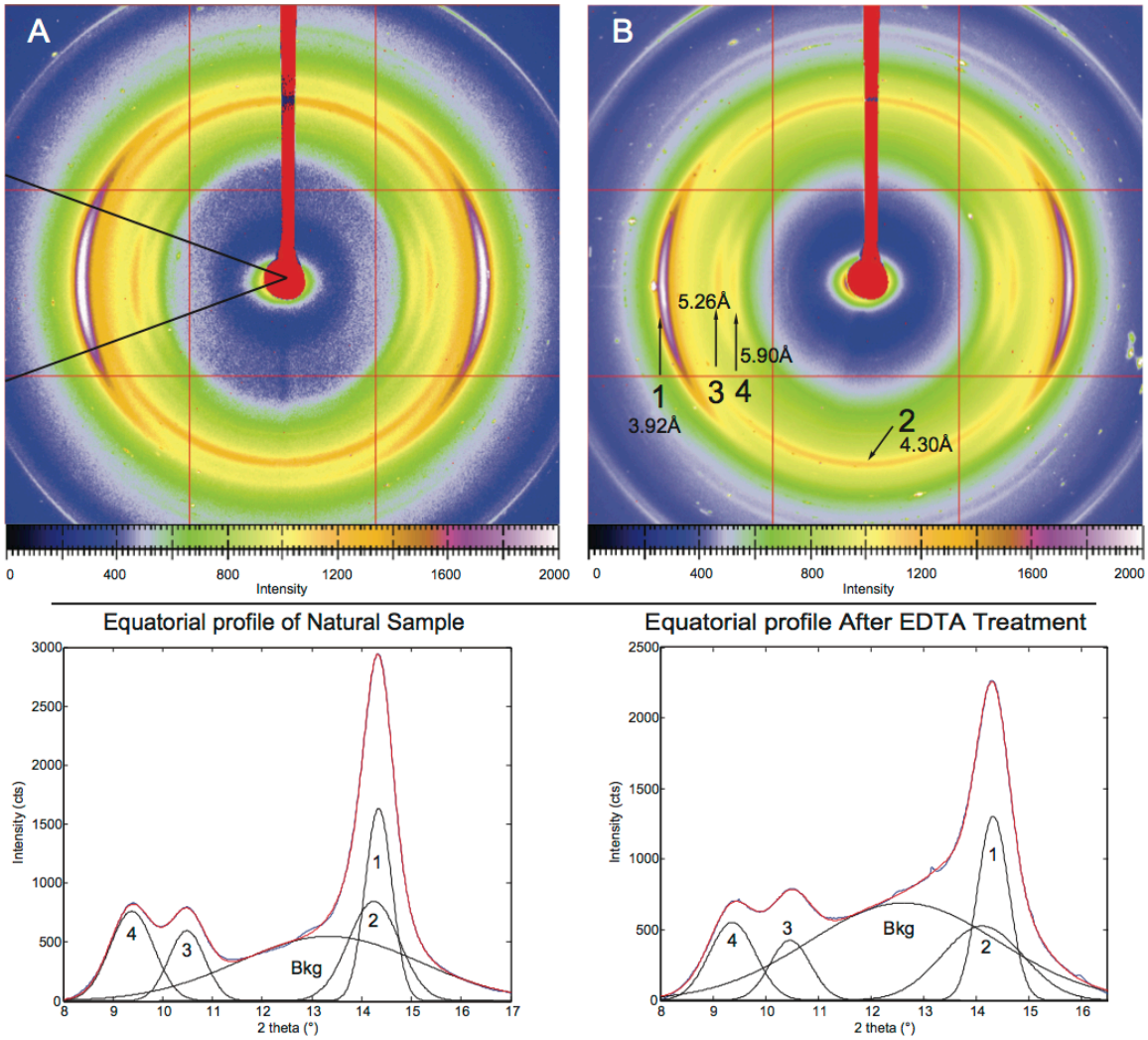

Figure 6. Wide Angle X-ray Diffraction (WAXD) of axially aligned caddisfly silk before (A) and after (B) EDTA chelation treatment. Integrations from the equatorial wedges are shown below each profile and the data were fit to a combination of Gaussian peaks to extract the nanocrystalline and amorphous fractions. Following the EDTA treatment the crystallinity decreases and amorphous content increases due to disruption of the b-sheet structure through cation chelation.

A comaprison of WAXD data before and after the EDTA treatment (see Figure 6) revealed a significant decrease in nanocrystallinity (~15-25%) while, the amorphous fraction increased correspondingly (~20%). This is consistent with the chelating agent disrupting the β-sheet structure by removing the cations that stabilize the phosphorylated Ser-rich structures (see Figure 4).

In addition to using SEM and WAXD to probe morphological and structural changes to the caddisfly silk, we also probed the phosphorylated Ser environment with ^{31}P MAS solid-state NMR. Initially, both ^{31}P direct detect (DD-) MAS and cross poalrization (CP-) MAS spectra were collected for caddisfly silk in its native, hydrared state. The ^{31}P solid-state NMR data provide clear evidence for rigid phosphate local environments in native caddisfly silk even in the presence of water. Both the DD-MAS and CP-MAS spectra in panels A and B of Figure 7 exhibit broad MAS powder patterns with an isotropic ^{31}P chemical shift of 1.5 ppm. The ^{31}P

Chemical Shift Anisotropy (CSA) pattern mapped by the spinning sidebands exhibits a negative skew parameter of -0.4 which is indicative of a rigid phophate carrying a net charge of -2. One might expect charged phosphoserine residues to be highly mobile and water solvated however, observation of a strong ^{1}H-^{31}P CP-MAS signal implies that the phosphates are surrounded by a rigid, strogly dipolar coupled network. EDTA-treatment clearly disrupts this rigid phospahte environment making the domain mobile as evidenced by complete loss of CP-MAS signal and a sharp isotropic DD-MAS resonance. Post trreatment of the fiber with CaCl2 recovers some of the rigid phosphorylated β-sheet Ser-rich structure. See Figure 8 for a molecular model of b-sheet diruption by EDTA chelation and reversible rigid b-sheet recovery following $CaCl_2$ post treatment. For more info on this work see *Biomacromolecules*. **2014**, *15*, 1269.

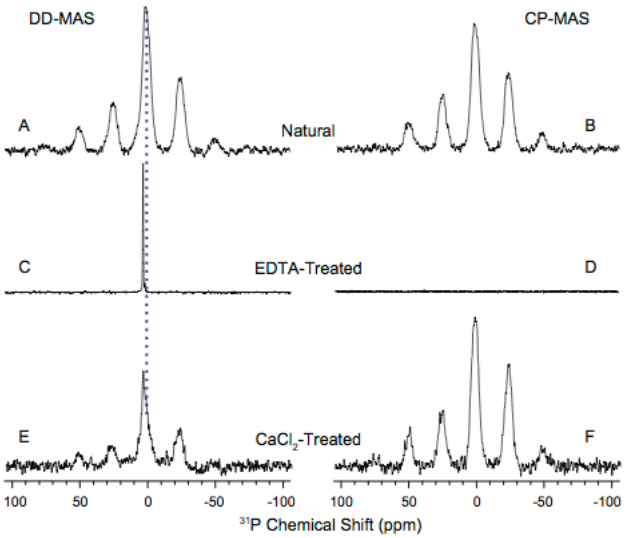

Figure 7. ^{31}P DD-MAS and CP-MAS NMR spectra on native, hydrated (A, B), EDTA-treated (C, D) and $CaCl_2$-treated (E, F) caddisfly silk fibers. The EDTA treatment disrupts the phosphorylated β-sheet Ser environment making it mobile. A post $CaCl_2$ treatment recovers some of the rigid phosphorylated β-sheet structure.

Another animal silk that we began investigating durring year one of funding is silk produced by Embiopterans or webspinners. Webspinners are social insects that procuce silken galleries and sheets in which they live and breed using an exceptionally fine silk with only 90-100 nm diameters. We have used a combination of techniques including electron microscopy (EM), Fourier transform infrared (FT-

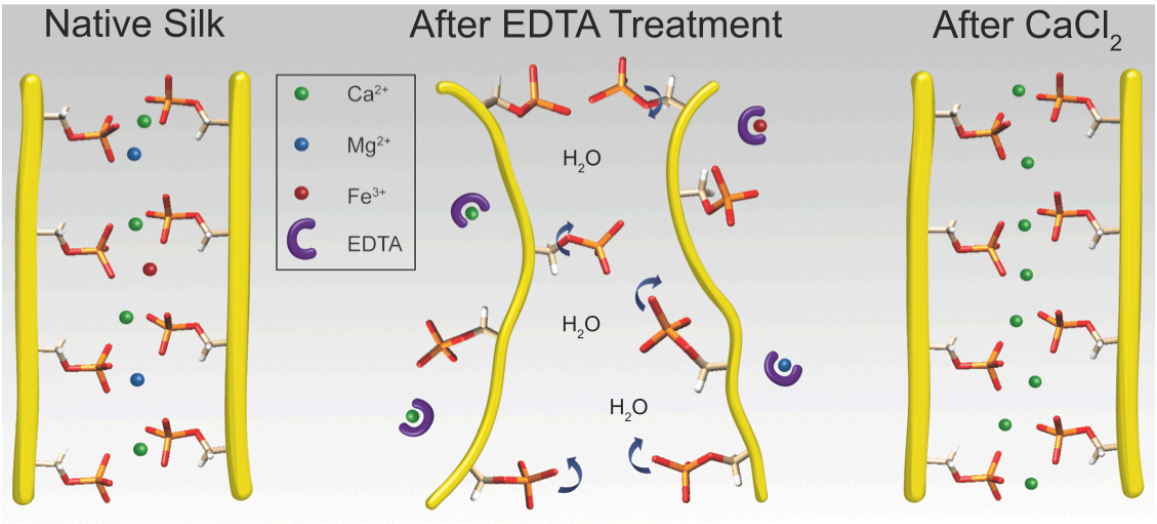

Figure 8. WAXD and ^{31}P solid-state NMR data illustrate that divalent cation stabilized phophoserine β-sheet structures can be disrupted through EDTA chelation and reversibly re-formed following a $CaCl_2$ treatment.

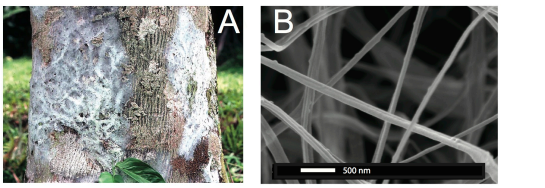

E

Webspinner fibroin repetitive regions

Sequence	Species
GAGSGSGAGSGSGAGSGAGSGSGAGSGSGA	*Antipaluria urichi*
GSGHGSSSSSSGDGSGSGSGSGSGSGSGS	*Aposthonia ceylonica*

Figure 9. (A-D) Optical and SEM images of arboreal embioptera silk from the species *Antipaluria urichi*. The webspinners work communally producing silken sheets and tunnels that protect and harbor the colony (A) using exceptionally fine (~90 nm) silk fibers (B, C) extruded from their tarsus (forearm) indicated with arrows in (D). The repetitive primary amino acid sequence is shown for two species, *Antipaluria urichi* and *Aposthonia ceylonica*. Sequences were obtained from GenBank [FJ361212] and [EU170437].

probe the secondary protein structure and nanocrystallinity.

WAXD data for webspinner silk collected from *Antipaluria urichi* is shown in Figure 10. The diffraction pattern of webspinner silk closely resembles our previously published spider silk diffraction patterns, confirming the presence of regular nanocrystalline β-sheet structures within the protein core. Careful analysis of the WAXD profile gives the crystallite size, orientation of nanocrystallites with respect to the fiber axis and the overall percent crystallinity. The radial broadening of the of the crystalline reflections was used to calculate the crystallite size along the a, b and c axes using Scherrer's equation. This resulted in crystallite dimensions of 3, 4 and 5 nm in the a, b and c axes, respectively. The IR) spectrosocpy, WAXD and ^{13}C solid-state NMR to probe the molecular level strcuture of the proteins that comprise webspinner silks from two species *Antipaluria urichi* and *Aposthonia ceylonia*. Optical and SEM images of arboreal embioptera insect silk from the species Antipularia urichi is shown in Figure 9 along with the webspinner silk portein repetivive primary amino acid sequence. The webspinner silks primary amino acid sequences are extremely similar to the sequence of the *Bombyx Mori* silkworm with runs poly(Gly-Ala) that also contain Ser. These regions are know to form the nanocrystalline β-sheet structure that is the hallmark of silkworm silks. Our initial hypothesis was that similar β-sheet structures were present in webspinner silks and we used a combination of techniques to

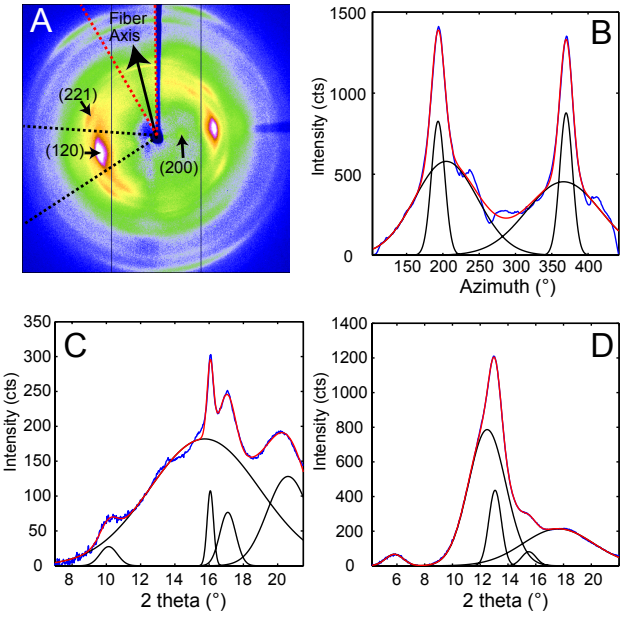

Figure 10. Summary of WAXD data for silk collected from *Antipaluria urichi*. Equartorial reflections (120) and (220) are associated with nanocrystalline b-sheets and the (221) reflection is due to the amorphous component. This webspinner silk has a very high crystallinity of 69%.

overall crystallinity was determined from the WAXD data to be 69%. This high crystallinity is likely due to the high fraction of Ser-rich poly(Gly-Ala) motifs in the webspinner silk protein.

^{13}C solid-state NMR data was collected for the webspinner silks to determine the secondary structure of the silk protein and identify the residues that are incorporated in the β-sheet nanocrystalline domains. In addition, a model peptide mimic, $GSGHG(S)_7GDG(SG)_7A$ based on the primary amino acid sequence for the *Ap. Ceylonica* webspinner silk was synthesized with FMOC chemistry and analyed by solid-state NMR. The peptide was lyophilized in a random coil structure and crystallized into a β-sheet structure with formic acid and the results compared with native webspinner silks. This ^{13}C CP-MAS solid-state NMR data is presented in Figure 11. The ^{13}C solid-state NMR spectrum of the webspinner peptide silk mimic in b-sheet structure is very comparable to the native webspinner silk (see Figure 11A). The serine Cβ resonance exhibits a ^{13}C isotropic chemical shift of 64.5 ppm which agrees well with a β-sheet conformational structure. Peak shifts and linewidths from the petide mimic in different structures were used to constrain the fitting the Ser Cβ resonance to quantify the population of seryl residues in β-sheet and random coil (amorphous) structures. These fitting results are shown in Figure 11B and illustrate that 70% of the Ser are in a b-sheet conformation compared to a 30% amorphous fraction. Interestingly, the 70% Ser β-sheet fraction compares very well with the 69% crystallinity determined from WAXD data (Figure 10). Thus, good agrrement is observed between the two techniques and provide strong indication that the nanocrystalline domains are Ser-rich β-sheet structures. For more info on this work see *RSC Advances* **2014**, *15*, 41301.

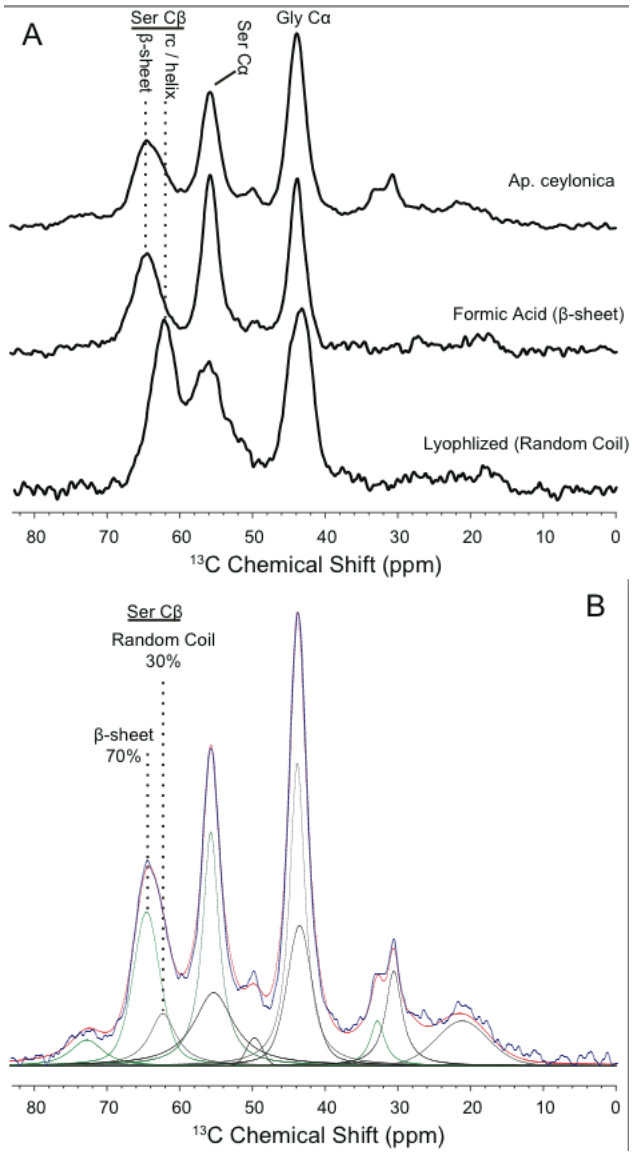

Figure 11. (A) ^{13}C CP-MAS NMR data of native webspinner silk (*Ap. ceylonica*) and the lyophilized model peptide in random coil and formic acid β-sheet form. (B) The native webspinner ^{13}C solid-state NMR spectrum was fit to determine that 70% of seryl residues adopt a β-sheet structure in good agreement with the crystallinity determined by WAXD.

Throughout the first year of funding we continued to work on developing Magnetic Resonance Imaging (MRI) with localized ^{1}H NMR spectroscopy to probe the spider silk producing process *in vivo*. We successfully imaged the major ampullate silk producing glands of a *Nephila clavipes* (Golden Orb Weaver) spider and conducted localized ^{1}H NMR spectroscopic mapping from the tail of the gland toward the beginning of the duct region. The results of these experiments are summarized in Figure 12. A MRI image of the *N. clavipes* major ampullate gland is shown in Figure 12A along with a red line indicting where localized ^{1}H NMR spectra were collected. Spectra were collected each mm along a 7 mm span from the gland tail where the spider silk proteins are synthesized to the beginning of the duct entryway. A representative ^{1}H NMR spectrum is shown in Figure 12B. Unfortunately, no dicernable change was observed in the ^{1}H isotropic chemical shift of the amide (NH), aromatic (Tyr) or Gln sidechain groups through the gland. This seems to indicate that there is no changes to the silk proteins secondary structure throughout the major ampullate gland and the narrow NH chemical shift (~0.5 ppm) indicates that the silk protein remains random coil throughout the gland with no evidence for any protein folding. Attempts to collect spectra from the duct regions were unsuccessful as the amount of fluid in the narrow duct provided insufficient signal to noise (S/N). In year 2, we moved in a new direction where we conducted MRI with localized ^{1}H NMR spectroscopy on silkworms. Silkworms are larger organisms compared to spiders with overall larger silk producing glands and we are hopeful that spectra can be collected from the glands and ducts. See preliminary data and discussion of these experiments below.

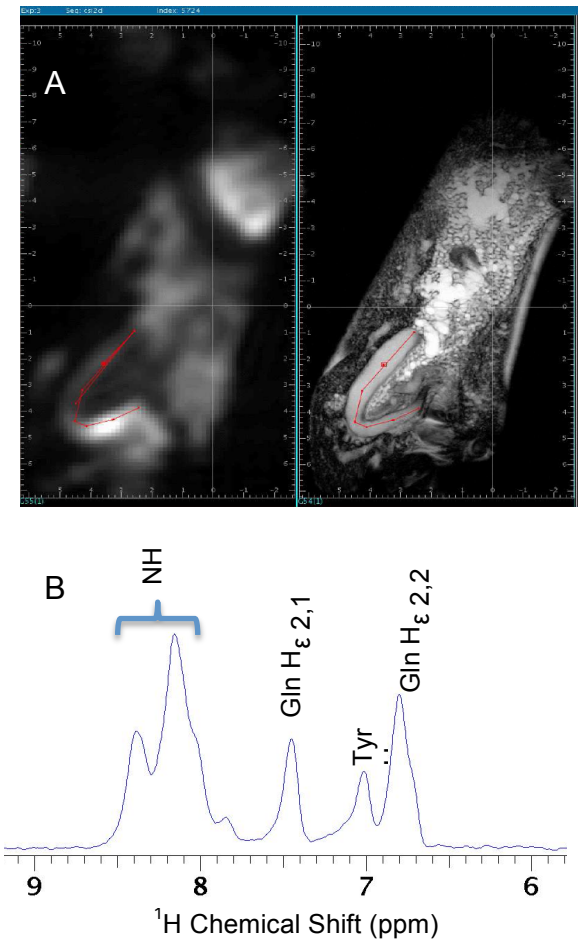

Figure 12. Summary of MRI data with localized ^{1}H NMR spectroscopy for *N. clavipes* spider. (A) MRI images of the spider's major ampullate gland. The red line indicates where localized ^{1}H NMR spectra were collected each mm along the gland from the gland tail where the silk proteins are synthesized to the beginning of the duct region. Spectra were collected each mm for 7 mm through the gland. No discernable change in the ^{1}H NMR spectrum was observed. (B) A representative localized ^{1}H NMR spectrum with resonance assignment.

4.2 Accomplishments/New Findings (Year 2):

In the year 2 funding period**,** we expanded our 2D ^{2}H-^{13}C HETCOR MAS NMR experiments to investigate the Ala-rich regions of spider dragline silk from *Nephila clavipes* spiders. 2D ^{2}H-^{13}C HETCOR MAS solid-state NMR Data for $^{2}H/^{13}C/^{15}N$-Alanine labeled major ampullate (dragline) spider silk is displayed in Figure 13. The data illustrates the site-specific nature of the ^{2}H quadrupole line shapes extracted from the 2D HETCOR MAS NMR experiments. The extracted site-specific Ala $^{2}H\alpha$ and $^{2}H\beta$ quadrupole line shapes are displayed in Figure 13. ^{2}H quadrupole patterns correlating to the two different Cβ resonances (17.4 and 20.9 ppm) are identical, indicating that Ala $^{2}H\beta$ present in the β-sheet and 3_1-helical regions possess the same quadrupole line shapes. ^{2}H quadrupole line shape simulations were conducted and compared with experimental data to interpret the dynamics for these regions. As shown in Figures 13B and C, the Ala methyl deuterium motion is consistent with a three-site reorientation along the C_{3V} axis in the fast motion regime ($>10^{8}$ s^{-1}) as expected. In addition, the experimental Ala $^{2}H\alpha$ line shape agrees well with a static MAS pattern (Figures 2D and E), illustrating the rigidity of the local backbone environment ($< 10^{2}$ s^{-1}) for Ala-rich regions in dry, native dragline silk.

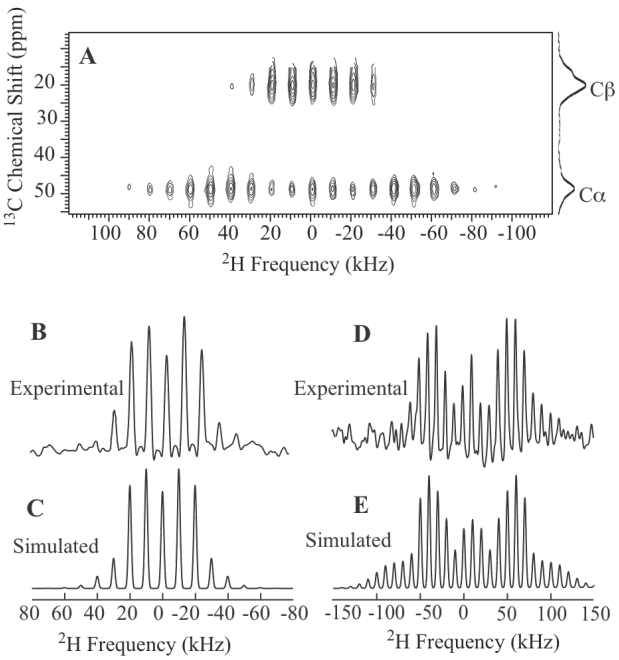

Figure 13. (A) ^{2}H-^{13}C HETCOR MAS NMR spectrum for *N. clavipes* dragline silk collected from spiders fed with U-[$^{2}H_4$,$^{13}C_3$,^{15}N]-Ala aqueous solution. Rotor spinning frequency is 10 kHz. (B) Ala $^{2}H\beta$ quadrupole line shapes extracted from the 2D spectrum. (C) Simulated ^{2}H quadrupole line shape for methyl deuterium undergoing three-site reorientations about the C_{3V} symmetry axis in the fast motion regime ($>10^{8}$ s^{-1}). (D) Ala $^{2}H\alpha$ quadrupole line shape extracted from the 2D spectrum. (E) Simulated ^{2}H quadrupole line shape for rigid ($<10^{2}$ s^{-1}) deuterium. All simulations were conducted using the SPINEVOLUTION software package.

When the $^{2}H/^{13}C/^{15}N$-Alanine labeled major ampullate (dragline) spider silk is wet (supercontracted), signal losses were observed for both Ala Cα and Cβ in the ^{2}H-^{13}C CP-MAS experiments (see Figure 14). No Ala Cβ signal is observed for the 3_1-helical motifs because they become extremely mobile when in contact with water resulting in inefficient CP between ^{2}H and ^{13}C. In addition, the previously reported Ala 3_1-helical content is 18% for *N. clavipes* dragline silk, which cannot explain the 31% Cα and 34% Cβ signal loss observed in 1D CP-MAS spectrum when the silk is wet and supercontracted. Previous NMR and XRD studies by our group and others indicated that the secondary structure of the Ala-rich β-sheet region

in spider dragline silk remains in tact upon supercontraction. Thus, there must be a CP signal loss due to Ala present in β-sheet regions that interact with water in wet silk.

We also used ^{13}C-detected Ala ^{2}Hβ relaxation data to further exhibit the presence of two components in the Ala-rich β-sheet domains. The Ala ^{2}Hβ T_1 for one component is 38 ms and 569 ms for the other (Table 1). This agrees with the existence of two different β-sheet components indicated by the Ala ^{2}Hβ T_1 measurement for dry, native silk. According to the relation between T_1 and motional rate, three-site reorientation rates for Ala deuterated methyls in wet silk was determined to be 5×10^{9} s^{-1} and 7×10^{10} s^{-1} for the two components, respectively. Based on the T_1 data fit, the population for the two components is 84% and 16%, respectively. Comparing with dry silk, a lower percentage was found for the component possessing a longer T_1 (higher Ala ^{2}Hβ reorientation rate) in wet, supercontracted silk. This can be explained by this component exhibiting a lower CP efficiency due to the existence of additional mobility when silk proteins interact with water compared to the other component. This is a result of the local backbone motion as discussed below. Thus, the ratio of Ala residues residing in the two components of the β-sheet domains is 55:45 based on T_1's measured for dry silk. In addition, due to the non-detectable CP signal, ^{2}H T_1 could not be determined for Ala residues present in 3_1-helical regions for the wetted silk.

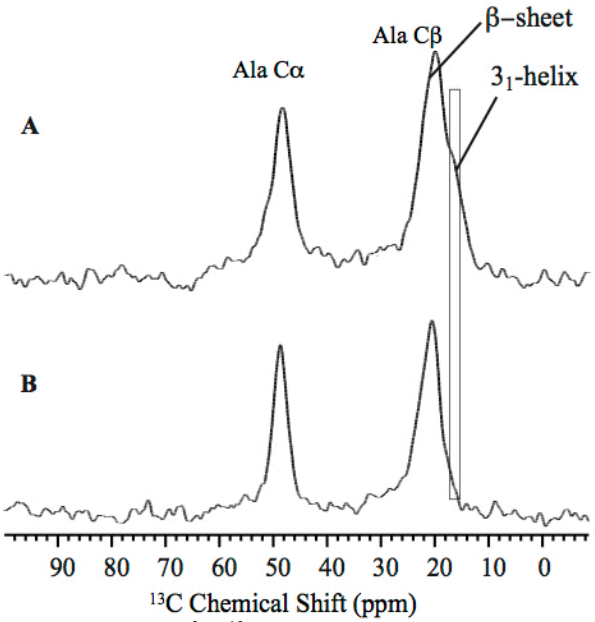

Figure 14. 1D ^{2}H-^{13}C CP-MAS spectrum for (A) dry and (B) wet, supercontracted *N. clavipes* dragline silk collected from spiders fed with U-[$^{2}H_4$,$^{13}C_3$,^{15}N]-Ala aqueous solution. Two Cβ chemical shifts, 20.9 and 17.4 ppm, are observed as shown in the figure, corresponding to Ala residues locate in β-sheet and 3_1-helical regions in silk proteins.

Table 1. Ala ^{2}Hβ spin-lattice relaxation times for *N. clavipes* dragline silk fibers. The values are extracted from fits of ^{2}H relaxation data.

silk sample	β-sheet		3_1-helical
	component 1 T_1 (ms)	component 2 T_1 (ms)	T_1 (ms)
dry, native	24	157	35
wet, supercontracted	38	569	—

1D ^{2}H solid-echo and one-pulse NMR experiments were conducted for dragline silk in both the dry and wet, supercontracted states. Compared to the dry silk, a significantly decreased signal was observed for the wet silk (Figure 15A). The center peak does not show signal increase in the spectrum of wet silk, ruling out the possibility that the signal decrease was caused by the deuterons becoming isotropic. Further, for wet

silk, the ^2H center band and ±1/2 spinning sidebands clearly exhibit much broader line widths, especially at ≤10% peak height (Figure 15A). For example, the center peak shows a line width at 5% peak height that is three times as large as that of dry silk (Figure 15A). This indicates the existence of a ^2H quadrupole pattern having broad peak widths in wetted silk.

In order to extract all ^2H components, a peak fitting routine was implemented for 1D ^2H spectrum of both dry (Figure 15B) and wet silk (Figure 15C). A motionally averaged ^2H quadrupole line shape and a rigid ^2H pattern were extracted from the fits. The motionally averaged ^2H line shape could be assigned to Ala Hβ and the rigid ^2H pattern to Ala Hα, Gly Hα and Glx Hα/β. Compared with dry silk, 50% signal (integral) loss is observed for the wet, supercontracted silk for ^2H solid-echo experiments for the extracted Ala $^2H\beta$ component that possesses the classical fast three-site reorientation methyl deuterium pattern (see Figure 15B1 and 15C1). The signal loss for this component is 55% in a one-pulse experiment. In addition, fitting residuals of ^2H spectra indicate the presence of positive broad peaks for supercontracted (wet) silk (Figure 15C3). This differs from the case of dry silk, where fitting residuals have intensities close to zero with several outlier points caused by an imperfectly phased experimental spectrum (see Figure 15B, C and D). Thus, the decreased Ala $^2H\beta$ signal could be explained by the molecular dynamic changes for a portion of the deuterons when silk proteins interact with water. The corresponding molecular dynamics leads to a ^2H MAS quadrupole pattern consisting of much broader peaks and a significantly reduced ^2H spin-spin relaxation time (T_2). The peak line width of the ^2H MAS quadrupole pattern is 1.2 kHz according to the fitting residual shown in Figure 15C3. ^2H line shape simulation suggests that such a broad ^2H quadrupole pattern could only be a consequence of motion on the microsecond timescale (10^6 s^{-1}). Thus, the corresponding Ala methyl deuterium in the supercontracted dragline silk must include an additional microsecond molecular motion in addition to the fast three-site methyl reorientation. Here, a simple model is used to represent this motion, where the entire methyl group reorients between two sites separated by 80°±10° along an external axis (Figure 15E). Considering Ala contains no additional bond on the side-chain to serve as a reorientation axis for the methyl group, the reorientation axis must be the local backbone axis. Therefore, this microsecond motion is the local backbone reorienting along its long axis. Overall, this can be simulated by the local backbone undergoing anisotropic reorientation at two sites separated by 80°±10° along its long axis with a rate of 1×10^6 s^{-1} (Figure 15E). Here, according to the signal loss observed for the three-site reorientating $^2H\beta$ pattern, Ala residues possessing such microsecond backbone motion account for 50-55%. This type of Ala is likely located in two different domains - 3_1-helical motifs and partial β-sheet regions. The β-sheet region portion should be one of the two components identified by the T_1 measurements as discussed above.

As discussed above, two types of motifs are distinguished with different molecular dynamics for β-sheet domains in spider dragline silk proteins. Here, we use β-sheet sub-region 1 and 2 to refer to the domains with slower and faster molecular motions, respectively. Based on the ^2H T_1 measurement as discussed above, the ratio between β-sheet su-region 1 and 2 is 55:45. Further, 1D 2H signal loss observed for wet, supercontracted silk indicates that the sum of Ala residues in β-sheet sub-region 2 and 31-helical motifs account for 50-55%. Considering Ala residues are only present in β-sheet and 3_1-helical structures in silk protein repetitive domains, the percentage of Ala in

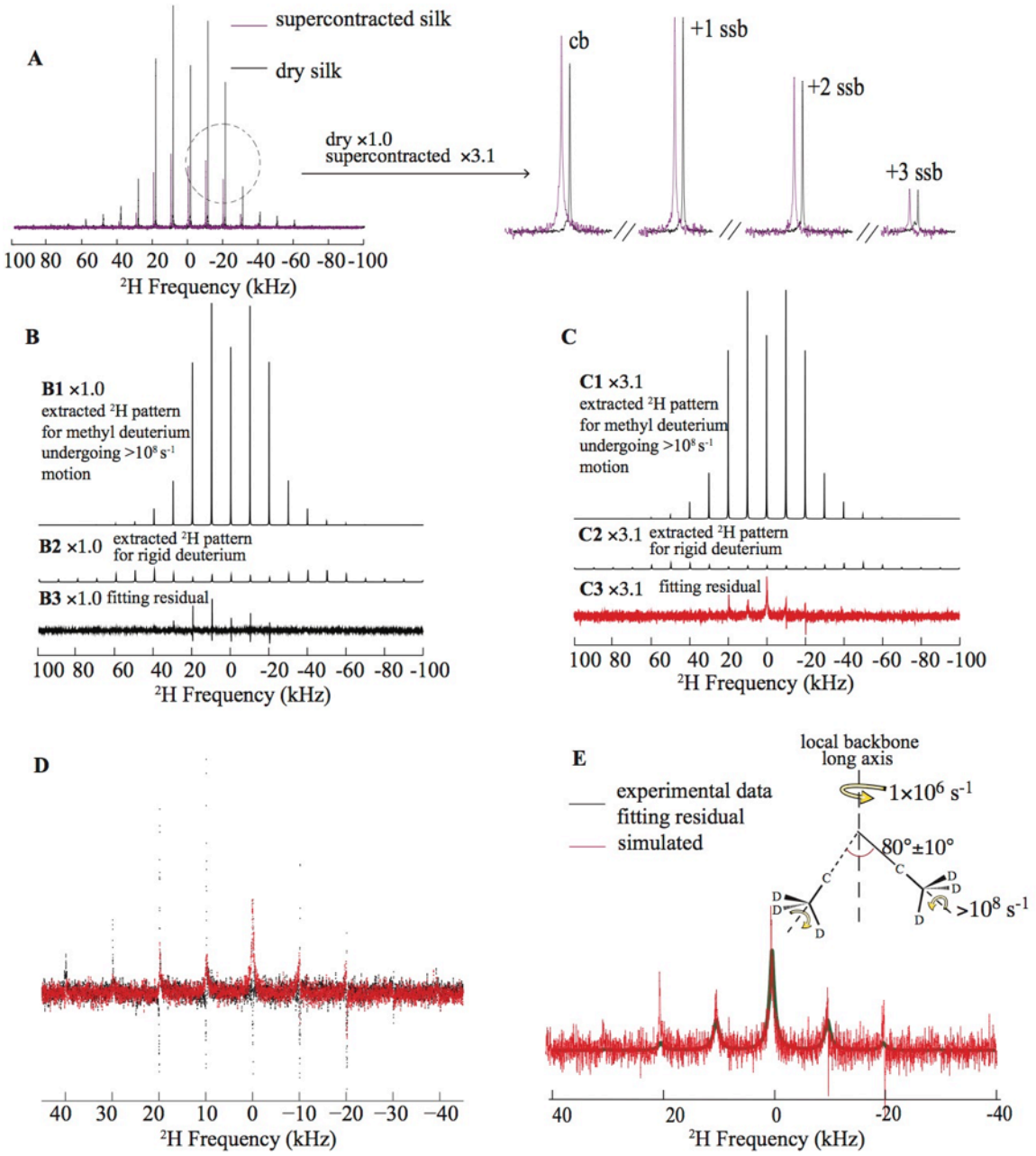

Figure 15. (A) ^{2}H solid-echo MAS spectra for *N. clavipes* dragline silk collected from spiders fed with U-[$^{2}H_4$,$^{13}C_3$,^{15}N]-Ala aqueous solution. Centerband (cb) and +1/2/3 spinning sidebands (ssb) are expanded and shown on the right for comparison. The spectrum of supercontracted silk is slightly shifted to the right in the figure for better visualization. (B) and (C) ^{2}H solid-echo spectrum fit for dry and supercontracted silk, respectively. Peak fitting was performed using DMFit. (D) Stacked line scatter plot of the fitting residuals for dry (black) and supercontracted (red) silk. Same vertical scale was used for the two spectra. (E) Experimental (black) and simulated (red) Ala $^{2}H\beta$ line shapes. The experimental data is the fitting residual of supercontracted silk shown in C and D. Simulation was performed for methyl groups with a particular molecular motion - the entire methyl group undergoing reorientation between two sites at an angle θ with a rate k while each deuterium undergoes fast three-site reorientation about the C_{3V} symmetry axis. The simulated spectrum shown in the figure is obtained with θ=80°±10° and k=1×10^{6} s^{-1}. The schematic representation for the motion is displayed on the upper right. Simulations are conducted using SPINEVOLUTION.

β-sheet sub-region 1, 2 and 3_1-helical regions is 45-50%, 37-40% and 10-18%, respectively. The local backbone and side-chain motional timescale were determined with ^2H MAS NMR for the three Ala-rich regions of the silk proteins and are summarized in Table 2.

Table 2. Protein local backbone and side-chain dynamics for Ala-rich regions in *N. clavipes* dragline silk fibers in the dry and wet, supercontracted states.

		β-sheet sub-region 1	β-sheet sub-region 2	3_1-helical region
Ala percentage		45-50%	37-40%	10-18%
dry, native	**backbone**	$<10^2$ s^{-1}	$<10^2$ s^{-1}	$<10^2$ s^{-1}
	side-chain	3×10^9 s^{-1}	2×10^{10} s^{-1}	$4.5\times10^9 s^{-1}$
wet, supercontracted	**backbone**	$<10^2$ s^{-1}	1×10^6 s^{-1}	1×10^6 s^{-1}
	side-chain	5×10^9 s^{-1}	7×10^{10} s^{-1}	$>4.5\times10^9 s^{-1}$

Previous solid-state NMR studies of spider dragline by our group and others have shown that poly(Ala) and poly(Gly-Ala) form the β-sheet nanocrystalline structures. It is noted from the MaSp1 primary sequence that poly(Gly-Ala) motifs are located between poly(Ala) and the disordered helical domains. This specific interfacial position makes the poly(Gly-Ala) motifs undergo faster motion compared to the poly(Ala) β-sheet core domains. Thus, it is logical to assign poly(Gly-Ala) and poly(Ala) domains to β-sheet

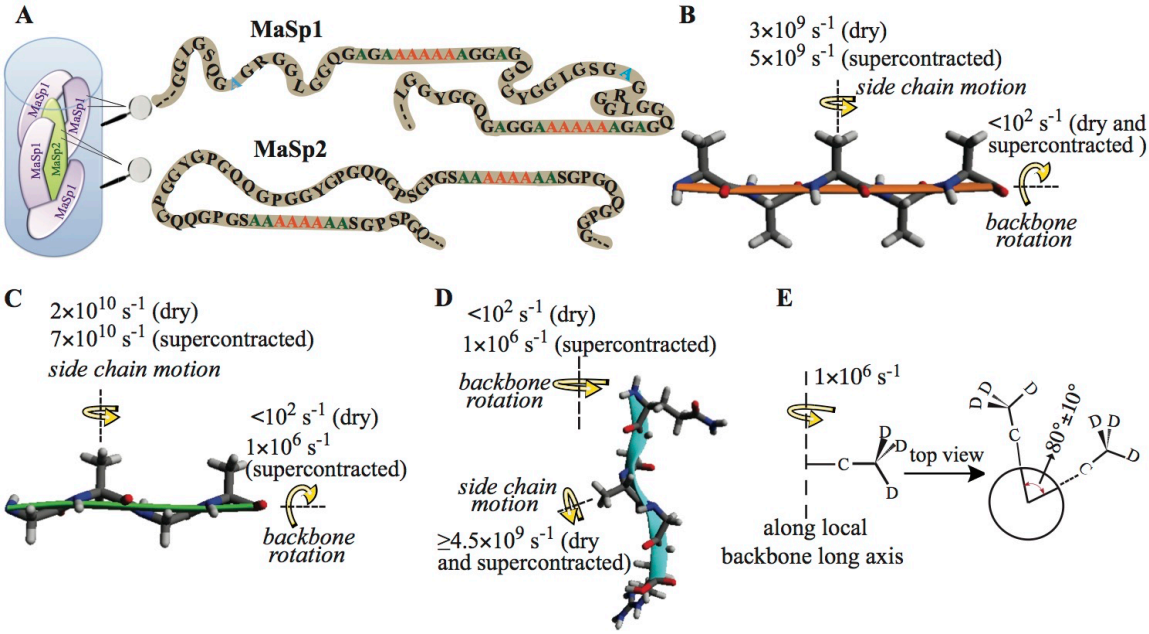

Figure 16. Silk protein backbone and side-chain dynamic model for *N. clavipes* dragline silk in dry and wet, supercontracted states. (A) Primary amino acid sequences for MaSp1 and MaSp2 repetitive motifs. Ala residues are highlighted for β-sheet sub-region 1 (orange), β-sheet sub-region 2 (green) and 3_1-helical region (cyan). (B) Molecular dynamics model for β-sheet sub-region 1. (C) Molecular dynamics model for β-sheet sub-region 2. (D) Molecular dynamics model for 3_1-helical region. (E) The side view and top view (looking down the backbone direction) of the backbone rotation for β-sheet sub-region 2 and 3_1-helical region in wet (supercontracted) silk. It is the rotation along the local backbone long axis represented by anisotropic reorientation between two sites separated by 80°±10° with a rate of 10^{-6} s^{-1}. The side-chain motion is Ala methyl deuterium undergoing three-site reorientations along the C_{3V} symmetry axis

sub-region 2 and 1 in MaSp1, respectively (see Figure 16 for structural model with dynamics determined by ^{2}H solid-state NMR). In MaSp2, poly-Ala β-sheet crystalline regions connect with flexible type II β-turn motifs. In this case, partial poly(Ala) motifs are located at the interfacial positions connecting the flexible regions and β-sheet core domains, and, exhibit faster molecular motions (see Figure 16).

β-sheet sub-region 1 and 2 is located in the β-sheet nanocrystalline domain and the interfacial position connecting the disordered helical and turn-like motifs, respectively. Thus, being impacted differently by the disordered motifs, the two regions present unique molecular dynamics in both dry and wet, supercontracted states. In dry (native) silk, the local silk protein backbone is static ($<10^{2}$ s^{-1}) for all Ala environments. When the silk is wet (supercontracted), β-sheet sub-region 2 and 3_1-helical domains exhibit microsecond local backbone reorientation because of interactions with water. Previous studies suggested that the β-sheet inter-chain hydrogen bonding is the dominant source of silk strength. Although the major structural features remain unchanged, the microsecond motion exhibited by β-sheet sub-region 2 could disrupt the inter-chain hydrogen bonding and concurrently help explain the decrease in stiffness for wet, supercontracted silk. In addition, water molecules mobilize and soften the helical regions when silk is wet, contributing to the observed the extensibility increase. Overall, the present work provides a structural and dynamic explanation for the decreased stiffness and increased extensibility observed for wet, supercontracted spider dragline silk. For more on this work, see *Biomacromolecules* **2015**, *16*, 852.

One of the most interesting results from our year 2 funding was the ability to grow spider silk fibers directly from the gland fluid in the laboratory at acidic pH and monitor the assembly kinetics with a ^{13}C MAS solid-state NMR approach developed by our research team. In this work, the impact of acidification on spidroin assembly was investigated for *Latrodectus hesperus* (Black Widow) native major ampullate (MA) silk gland fluid with an *in vitro* ^{13}C solid-state MAS NMR approach. The spider silk assembly process was investigated at a number of acidic pH

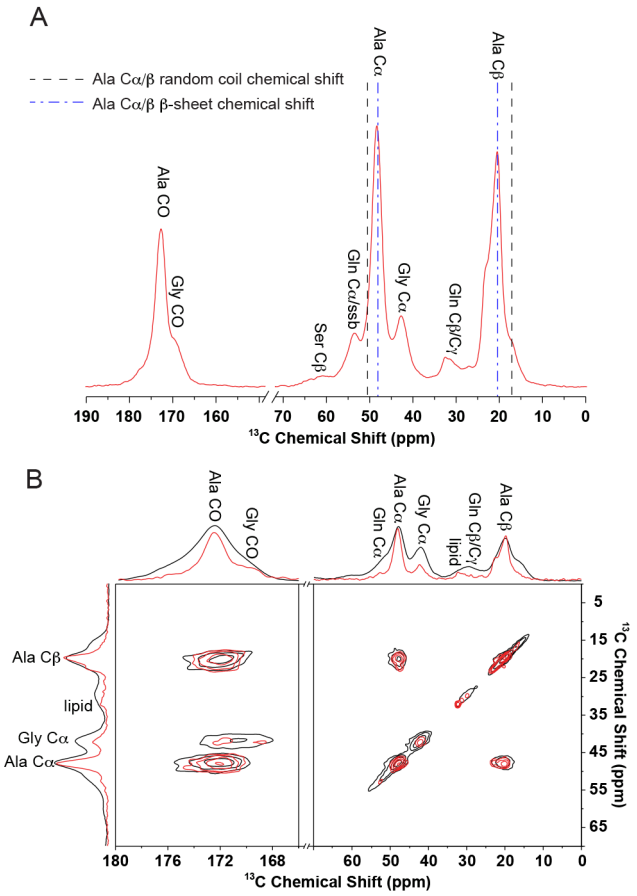

Figure 17. (A) 1D ^{1}H-^{13}C CP-MAS NMR spectrum and (B, red) 2D ^{13}C-^{13}C DARR spectra of U-^{13}C-L-alanine labeled BW MA gland fluid incubated at pH = 3 for 24 hours. The 2D ^{13}C-^{13}C DARR spectrum of the (B, black) U-^{13}C-L-alanine labeled BW dragline silk (B, black) is shown for comparison purposes. Note the similarity between the 2D spectrum for the incubated gland fluid and dragline spider silk.

conditions. Compared to other characterization techniques, this solid-state NMR method is able to resolve and detect poly(Ala) present in both the liquid (as random coil) and the solid phase (as insoluble β-sheet structures) during silk fiber assembly. The resulting kinetic data represents the first illustration of monitoring pH-dependent spider silk assembly kinetics *in vitro* at near native conditions with a NMR spectroscopic method. The assembly of spider silk fibers from the native MA gland fluid was observed for a range of pH from 3 to 6 with a long period for nucleation followed by a rapid pH-dependent elongation process.

2D ^{13}C-^{13}C dipolar assisted rotational resonance (DARR) experiments were conducted to compare the secondary structures between the aggregated spidroins from the acidified gland fluid with the spidroins in the native MA silk collected from the same spiders (see Figure 17B). The 2D ^{13}C-^{13}C spectra and extracted conformation dependent chemical shifts are strikingly comparable illustrating that the structures formed in the acidified gland fluid are similar to the structures formed in native spider silk fibers (see Table 3). In Figure 17B, the cross peaks for Ala and Gly from the aggregated silk gland fluid and silk fibers are overlapped and compare extremely well. The only difference in the spectra of the native spider silk and the acidified gland fluid is the lower intensity observed for resonances from disordered helical and turn-like domains dues to presence of water. Water penetrates these disordered domains increasing local molecular dynamics for these regions with a corresponding decrease in CP efficiency. This is similar to observations made in supercontracted spider dragline silk where the silk is wetted with water (see dynamic discussion above).

Table 3. ^{13}C chemical shift of native Black Widow MA silk gland protein before and after fiber formation (aggregated) at acidic pH, the chemical shifts for model peptides with known secondary structures are shown for comparison purposes.

	^{13}C Chemical Shift [a]					
	gland	aggregated	native silk	α-helical	β-sheet	random coil
Ala C_α	50.3	48.3, 49.7	48.6, 49.4, 52.4	52.3-52.8	48.2-49.3	50.5
Ala C_β	16.5	20.5, 16.6	20.4, 17.0, 16.4	14.6-16.0	19.9-20.7	17.1
Ala CO	175.5	172.2	172.4, 175.4	176.2-176.8	172.0-175.2	175.8
Gly C_α	42.9	42.3	41.3, 43.0		43.2-44.3	43.1
Gly CO	171.8	168.9, 171.9	168.8, 171.8		168.4-169.7	172.9
Gln C_α	53.4	53.3	52.4	56.4-57.0	51.0-51.4	54.2
Gln C_β	26.8	26.9	27.4	25.6-26.3	29.0-29.9	27.4
Gln C_γ	31.3	31.2	30.9	29.7-29.8	29.7-29.9	31.7
Gln C_δ	177.8	177.7	177.5			178.5
Gln CO	174.0	-	172.8	175.4-175.9	171.9-172.2	174.0

[a] All chemical shifts are referenced to TMS.

Optical microscopy and TEM experiments conducted on the acidified gland fluid extracted from the NMR sample at pH = 3 clearly confirm the formation of needle-like fibers 10-100 μm in length illustrating that acidification of the gland fluid results in the formation of spider silk fibers (see Figure 18A,B). Interestingly, the fiber diameters were measured to be 1.5 ± 0.7 μm using TEM (see Figure 18C) which is very close to the 2.2 ± 0.1 μm diameter of native BW dragline silk fibers (Figure 18D). The large aspect ratio of

the fibers formed from the silk gland fluid in the present study suggests that the β-sheet structures are likely to be aligned parallel to the fiber axis as in native spider silk. Although X-ray diffraction data on the fibers is still required to confirm the alignment of β-sheet nano-structures and determine percent crystallinity and crystallite size. However, the length of the fibers have made such studies challenging compared to native spider silks. We are continuing to attempt WAXD and SAXD experiments in year 3 and are hopeful we will have diffraction data on these laboratory grown fibers soon.

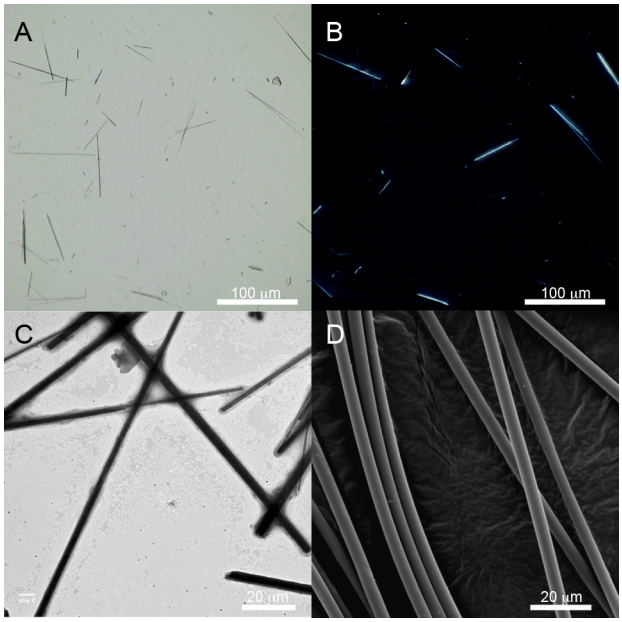

Figure 18. Polarized light microscopy images (A) with and (B) without cross-polars and (C) NS-TEM image for silk fibers assembled by incubating the BW MA silk gland fluid at pH = 3 for 24 hours. (D) SEM image of BW dragline silk fibers collected from the same spiders.

Different pH conditions ranging from 3 to 7 were investigated to study the impact of pH on spider silk assembly. At pH's below 7, the spidroins are assembled into an aggregated fiber with a β-sheet rich conformation. The overlay of the CP spectra at pH below 7 shows no obvious difference in secondary structures (data not shown). However, at pH = 6, the pH reported for the duct region of the spider silk gland and the dimerization of the N-terminal domain, an extremely long period of 7 days is required for the spidroins to self-assemble into the aggregated, fibrous state in the laboratory. In contrast, at more acid environments, the time it takes for the spidroins to aggregate can be greatly reduced to less than 24 hours.

The effect of pH on the spider silk spidroin assembly kinetics was monitored with fully relaxed ^{13}C DD-MAS solid-state NMR. For the unstructured spidroins, the ^{13}C DD-MAS spectrum exhibits relatively sharp peaks because of the fast sub-nanosecond silk protein backbone dynamics in the random coil state (see Figure 19). However, after the silk fiber is formed, broader peaks are observed with ^{13}C chemical shifts that correspond to β-sheet structures (see Figure 19). A time period of 24 to 35 hours was required to record the full process of spidroin assembly at different acidic pH conditions from 3 to 6. Consecutive ^{13}C DD-MAS spectra were collected with each one requiring 30 min to obtain quantifiable ^{13}C spectra with acceptable S/N ratio. The spider silk assembly transition is clearly monitored in the Ala C_β region of the spectrum where a simultaneous increase for the broad β-sheet resonance occurs with a corresponding decrease of the narrow random coil resonance (Figure 19). The fraction of Ala from the silk spidroins with different secondary structure (β-sheet or random coil) at each time point were determined by deconvoluting the Ala C_β region using typical peak fitting routines. To quantify the observed kinetic behavior of spider silk fiber formation and better analyze the impact of different pH conditions, a modified Kolmogorov-Johnson-Mehl-Avrami

(KJMA) kinetic model from the overall crystallization theory was applied to the experimental data. The general form of the analytical expression for the model is:

$$\alpha(t) = 1 - \exp\left[-\left(\frac{t}{\theta}\right)^n\right]$$

where α represents the normalized experimentally observed intensity for the Ala C_β random coil peak, θ is a time constant quantifying the time scale of fiber formation and n is a kinetic index indicating the rate of elongation. To accommodate the model to our experimental data, a slight modification as follows was made to enable applicability of fitting a decreasing sigmoidal curve with a non-zero fraction at equilibrium:

$$\alpha(t) = A + (1 - A)\exp\left[-\left(\frac{t}{\theta}\right)^n\right]$$

where an extra parameter, A, was added to better determine the percentage of Ala that did not adopt a β-sheet conformation at equilibrium and remained random coil. The lag time, t_l, and the maximal rate of elongation, k, can be determined based on the following formulas:

$$t_l = \left(\frac{n-1}{n}\right)^{\frac{1}{n}}\left[1 - \frac{e^{\frac{n-1}{n}} - 1}{n-1}\right]\theta$$

$$k = (n-1)\left(\frac{n}{n-1}\right)^{\frac{1}{n}} e^{-\frac{n-1}{n}}\frac{1}{\theta}$$

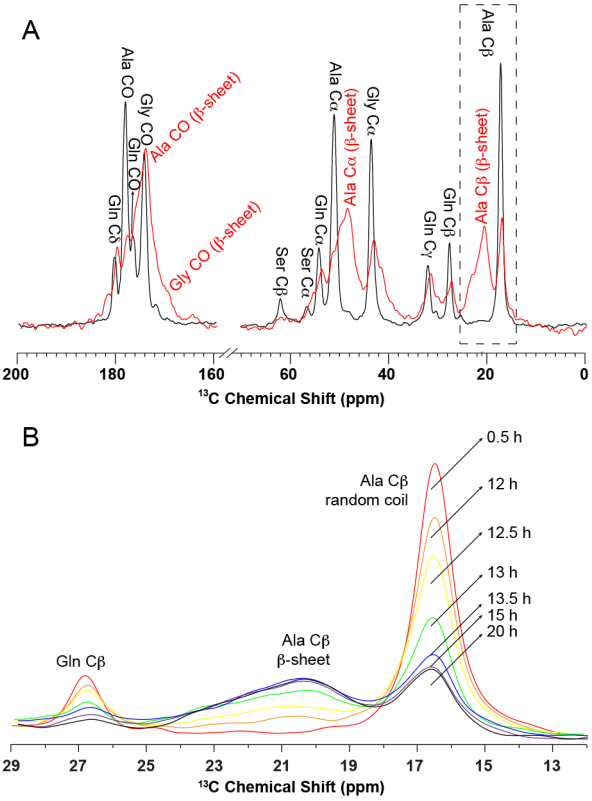

Figure 19. ^{13}C DD-MAS NMR spectra for U-^{13}C-L-alanine labeled BW MA silk gland fluid at pH = 4 (A, black) before and (A, red) after spider silk assembly (24 hrs). The Ala C_β region is framed by dashed lines and will be analyzed to monitor spider silk assembly kinetics. (B) Ala C_β regions from the ^{13}C DD-MAS spectra collected at different time from sample preparation are stacked illustrating that the decrease of the random coil resonance and increase of the β-sheet resonance can be observed simultaneously as a function of time.

The kinetic curves for spider silk assembly at different pH were established by plotting the normalized peak intensities of the random coil peak for the Ala C_β as a function of time. A signature sigmoidal shaped kinetic curve was observed for the spider silk assembly process for the three acidic pH's tested (see Figure 20) and the KJMA model fit the data very well. A long lag time was observed followed by rapid elongation indicating that nucleation is a prerequisite. The impact of pH on the different phases of spidroin fiber formation can be analyzed by applying the modified KJMA model to the kinetic curves (Table 4). At pH = 4, the shortest lag time (12.1 h) is required for the spidroins to shift to the rapid elongation phase. However, an extra 5.5 or 7 hours was observed for passing the nucleation phase at pH = 3 or pH = 5. Although the nucleation phase took a longer time at pH = 5, the β-sheet conformation yielded the largest

percentage (80%) of Ala in a β-sheet structure at equilibrium suggesting longer nucleation times are beneficial for the complete formation of crystalline β-sheet structures. However, the difference in the fraction of Ala that forms a β-sheet structure at different acidic pH's is small ranging from 70-80 % and not far off from the fraction of Ala in β-sheet structures from solid-state NMR studies conducted by our research group for native BW MA silk fibers where it was determined to be 88%. The increasing rate constants of the elongation phase from 0.24 to 0.91 with decreasing pH values from 5 to 3 indicates that the elongation process is accelerated by more acidic conditions.

The ^{13}C DD-MAS NMR spectrum of the BW spidroins within the MA glands displays narrow resonances with chemical shifts matching a random coil structure. Although the spidroins are stored in the silk glands at a near neutral but slightly acidic environment (pH ~ 6.3), a high concentration of NaCl (~180 mM) is present and believed to prevent premature aggregation and maintain an unstructured, random coil state. It has been proposed that an acidic pH gradient exists in the spinning system from the silk glands along the duct to the spinneret and is likely important for spider silk formation.

Table 4. Parameters extracted from the kinetic curves using a modified KJMA model for spider silk fiber assembly at different pH conditions and different MAS frequencies.

pH	n	θ	A	*k*	t_l
3 (4 kHz MAS)	45.5±3.6	18.4±0.1	0.22±0.01	0.91±0.07	17.7±0.1
4 (4 kHz MAS)	19.8±2.5	13.3±0.1	0.24±0.01	0.55±0.07	12.1±0.2
5 (4 kHz MAS)	14.2±0.5	21.8±0.1	0.20±0.01	0.24±0.01	19.2±0.1
4 (0 kHz MAS)	19.7±2.8	13.2±0.1	0.30±0.01	0.55±0.08	12.1±0.2

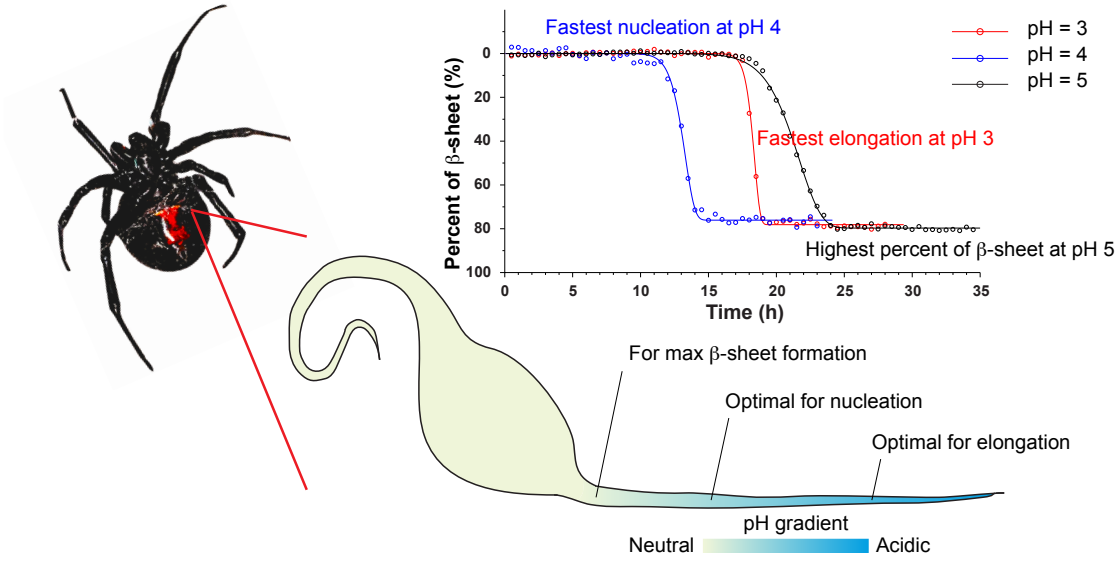

Figure 20. Kinetic curves for U-^{13}C-L-alanine labeled BW MA silk gland fluid incubated at pH = 3 (red circle), 4 (blue circle) and 5 (black circle). The solid curves were obtained by applying the modified KJMA model and the extracted kinetic parameters are shown in Table 4. A cartoon of the BW MA gland is shown below the data illustrating the acidic pH gradient in the duct and proposed influence of varying the pH on β-sheet content, nucleation and elongation.

With the limitation of experimental methods, accurate measurement to map out the pH values in the spinning system is still challenging. However, the spidroins are expected to experience much lower pH values near the spinneret. In addition, to induce fiber formation *in vitro* on the native spider silk gland fluid with a high NaCl content, a lower pH condition may be required compared to the *in vivo* spinning conditions. Therefore, to study the effect of acidic biochemical conditions on spider silk fiber formation, acidic conditions from pH = 6 to pH = 3 were investigated for the native BW MA spidroins. At pH = 7, the spidroins remain unstructured random coils for over 7 days with no evidence of aggregation, but when acidic conditions are applied, the metastable state of the unstructured spidroins is disturbed and aggregation to silk fibers occurs albeit with different kinetics. The spidroins assemble into fibers at pH ≤ 6, with no observable difference in the conformational structures of the folded spidroins for different pH values following fiber formation. However, distinguishable difference in the rates of fiber formation from 7 days at pH = 6 to 12 hours at pH = 4 are observed leading to the study on the kinetics of spidroin fiber formation at acidic conditions with ^{13}C DD-MAS NMR.

The kinetic profile of spidroin fiber formation is a typical sigmoidal curve. The long period of lag time indicates nucleation is required to allow further elongation. Unlike a parabolic curve, the sigmoidal curve also indicates no seeds existed in the system to help skip the nucleation phase. Because nucleation is a crucial prerequisite for fiber formation, it was important to determine that centrifugal and centripetal forces from MAS did not influence the kinetics to any appreciable extent as confirmed by the static ^{13}C NMR experiments (see Table 4). Comparison of the extracted kinetic parameter for static and 4 kHz MAS conditions illustrates that MAS has little impact on the spider silk assembly kinetics with the exception of a slightly higher remaining random coil fraction of 0.30 and 0.24 at equilibrium for the two conditions, respectively (data not shown).

The lag times observed for spider silk fiber formation as a function of pH in the present study are surprisingly long (> 12 hours) indicating that pH may not be the biochemical variable that controls nucleation. Previous studies on silkworm fibroins and spider spidroins indicate shorter lag times for fiber formation. These previous studies are likely not comparable to the investigation here because of the dilute (~ 0.1 % by wt) protein concentrations used compared to the much higher concentration of silk proteins (~23 % by wt) in the silk glands used in this study. Even though the remaining NaCl in the silk gland may postpone nucleation, the over 12 hours of lag time implies that other mechanisms may be responsible for nucleation. One possible explanation for this is the gel-like state of spider silk spidroins inside the MA gland that can prevent or postpone nucleation. Thus, any approaches to dissolve the dope inside silk glands will remove this stabilizing effect of the gel-like state with high salt content leading to faster aggregation due to increased hydrophobic interactions. Similarly, one must consider the other physicochemical influences such as dehydration, shearing forces and the influence of other ions that could be introduced in the duct to assist the nucleation process. We are in the process of looking at the impact of other cations and anions that are hypothesized to be introduced in the duct such as K+ and PO4-. These studies are on going and may play a role in the nucleation and overall silk fiber formation process.

As shown in Figure 6, the shortest nucleation phase was observed at a pH near the isoelectric point (pI = 4.25) of the N-terminal domains (NTD) of the spidroins. This result indicates the nucleation process may be related to the NTD. The NTD is known to

dimerize at pH = 6 and the dimerization becomes more stable as pH decreases. Compared to pH = 3 or 5, the solubility of the NTD dimer is much lower at a pH = 4. This is consistent with the results presented here where the shortest nucleation phase is observed at a pH = 4. In comparison, during the elongation process, the spidroins exhibit the fastest elongation rate at lower pH values. Since the pI of the entire silk protein was experimentally estimated to be ~ 4.2, the fastest rate of elongation phase at pH = 3 implies that the elongation phase is not governed by the solubility change of the entire silk protein. In addition, a larger percent of β-sheet structures is formed in the silk fibers with longer nucleation time. Combining the information listed above, it is reasonable to propose a possible model to explain the function of the pH gradient in the spinning system. The spidroins are initially stored in an unstructured, random coil state at near neutral pH, where the spidroins can remain stable. At pH = 6, the NTD first starts to form dimers followed by silk protein nucleation. Larger assemblies are formed at a pH ~ 5 to ensure higher percentage of β-sheet structures in the silk fiber, then the solubility of the silk protein drops dramatically at a pH = 4 leading to rapid fiber formation. When the dope is close to the spinneret, decreasing the pH below 4 can accelerate the elongation rate even further. Thus, a pH gradient can be used to regulate the speed of the nucleation and elongation as well as the final β-sheet composition in the spider silk assembly process. Lastly, although pH appears to be important in regulating and controlling spider silk assembly, the other physicochemical variables that have been discussed previously will certainly contribute to the assembly process and are being investigated in our laboratory with the described *in vitro* ^{13}C MAS solid-state NMR approach.

During year 2 funding we continued to work on developing MRI with localized ^{1}H NMR spectroscopy. As discussed above and shown in Figure 12 we have successfully developed and applied MRI with localized ^{1}H NMR spectroscopy to chemical shift map the major ampullate gland from the tail region where the silk proteins are synthesized to the beginning of the duct. We observed essentially no change in the ^{1}H spectrum including the amide protons (NH) that are sensitive to secondary structure. This indicates that the silk proteins remain unfolded, random coils throughout the gland environment with no evidence of protein folding into the hallmark β-sheet structure of spider silks. Unfortunately, attempts to collect localized ^{1}H NMR spectra for the narrow duct region, where many of the physiochemical changes responsible for spider silk formation are believed to occur, were unsuccessful because of the limited amount of material. In year 2 we decided to use this MRI approach with localized ^{1}H NMR spectroscopy to image and spectroscopically probe the silk glands of *Bombyx mori* silkworms. Silkworms have larger internal silk spinning systems compared to spiders and our hope is that we can have a better chance at collecting spectra from the duct region for these silk producing organisms. Our first MRI images and localized ^{1}H NMR spectra for the silkworm silk gland are shown in Figure 21. Similar to the silk protein in the spiders silk producing gland the silkworm silk protein is present in a random coil state similar to the results for the spider major ampullate gland shown in Figure 12. This shows that both silk producing organisms store the spider silk protein in the silk gland in an unstructured, random coil state. In year 3 of funding we plan to try to collect localize 1H NMR spectroscopy of the silkworm's duct region to see if this approach can detect in protein folding and silk formation within the organism *in vivo*.

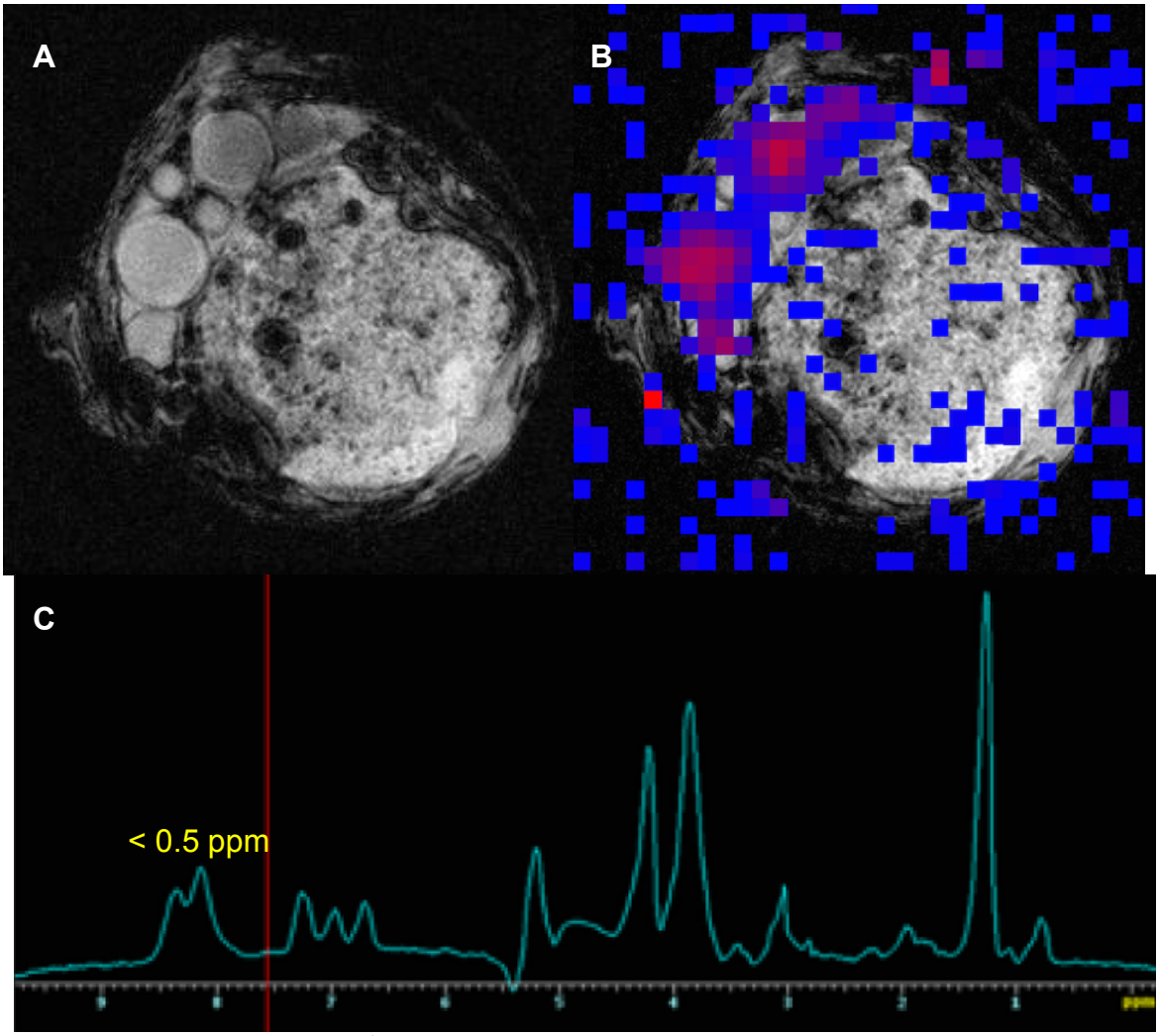

Figure 21. Summary of MRI data with localized ^{1}H NMR spectroscopy for *Bombyx Mori* silkworm. (A) MRI image of the silkworm's silk producing gland and (B) amide chemical shift mapping data. (C) A localized ^{1}H NMR spectrum from the silkworm silk gland. Note the small amide (NH) ^{1}H chemical shift range (<0.5 ppm) indicting that the silkworm silk protein is in an unfolded, random coil structure similar to the observations made in spiders (see Figure 12).

5. Personnel Supported:

1) Gregory P. Holland (PI), Supported one month of summer salary per year.

2) Jeffery L. Yarger (co-PI), Supported one month of summer salary per year.

3) Xiangyan Shi (Ph.D. Student, Research Assistant), Supported 3 months

4) Chengchen Guo (Ph.D. Student, Research Assistant), Supported 3 months.

5) Quishi Mou (Ph.D. Student, Research Assistant), Supported 3 months.

6) Dian Xu (Ph.D. Student, Research Assistant), Supported 15 months.

6) Forrest Thompson (Undergraduate Student, Part-time Researcher), Supported 500+ hrs.

6. Publications:

1) Shi, X., Yarger, J.L., Holland, G.P. "Elucidating Proline Dynamics in Spider Dragline Silk Fibre Using ^{2}H-^{13}C HETCOR MAS NMR" *Chem. Commun.* **2014**, *50*, 4856-4859.
2) Addison, J.B., Weber, W.S., Mou, Q., Ashton, N.N., Stewart, R.J., Holland, G.P., Yarger, J.L. "Reversible Assembly of β-sheet Nanocrystals within Caddisfly Silk" *Biomacromolecules* **2014**, *15*, 1269-1275.
3) Albertson, A.E., Teule, F., Weber, W., Yarger, J.L., Lewis, R.V., "Effects of Different Post-spin Stretching on the Mechanical Properties of Synthetic Spider Silk Fibers" *J. Mech. Behav. Biomed. Mater.* **2014**, *29*, 225-234.
4) Xu, D., Yarger, J.L., Holland, G.P., "Exploring the Backbone Dynamics of Native Spider Silk Proteins in Black Widow Silk Glands with Solution-state NMR Spectroscopy" *Polymer* **2014**, *55*, 3879-3885.
5) Tucker, C.L., Jones, J.A., Bringhurst, H.N., Copeland, C.G., Addison, J.B., Weber, W.S., Mou, Q., Yarger, J.L., Lewis, R.V., "Mechanical and Physical Properties of Recombinant Spider Silk Films Using Organic and Aqueous Solvents" *Biomacromolecules* **2014,** *15*, 3158-3170.
6) Addison, J.B., Osborn Popp, T.M., Weber, W.S., Edgerly, J.S., Holland, G.P., Yarger, J.L., "Structural Characterization of Nanofiber Silk Produced by Embiopterans (Webspinners)" *RSC Advances* **2014**, *4*, 41301-41313.
7) Sampath, S., Yarger, J.L., "Structural Hysteresis in Dragline Spider Silks Induced by Supercontration: An X-ray Fiber Micro-diffraction Study" *RSC Advances* **2015**, *5*, 1462-1473.
8) Shi, X., Holland, G.P., Yarger, J.L., "Molecular Dynamics of Spider Dragline Silk Fiber Investigated by ^{2}H MAS NMR" *Biomacromolecules* **2015**, *16*, 852-859.

9) Guo, C. Hall, G.N., Addison, J.B., Yarger, J.L., "Gold Nanoparticle-doped Silk Film as Biocompatible SERS Substrate" *RSC Advances* **2015**, *5*, 1937-1942.

10) Mou, Q., Benmore, C.J., Yarger, J.L., "X-ray Intermolecular Structure Factor (XISF): Separation of Intra- and Intermolecular Interactions from Total X-ray Scattering Data" *J. Appl. Cryst.* **2015**, *48*, 950-952.

11) Xu, D., Shi, X., Thompson, F., Weber, W.S., Mou, Q., Yarger, J.L., "Protein Secondary Structure of Green Lynx Spider Dragline Silk Investigated by Solid-state NMR and X-ray Diffraction" *Int. J. Biol. Macromol.* **2015**, *81*, 171-179.

12) Xu, D., Guo, C., Holland, G.P., "Probing the Impact of Acidification on Spider Silk Assembly Kinetics" *Biomacromolecules* **2015**, *16*, 2072-2079.

13) Mou, Q., Benmore, C.J., Weber, W.S., Yarger, J.L., "Insights into the Hierarchical Structure of Spider Dragline Silk Fibers: Evidence for Clustering of β-sheet Nano-crystallites" *Journal of Physics: Condensed Matter* **2015**, In Press.

7. Interactions/Transitions:

a. Participation/presentations at Meetings, Conferences, Seminars:

1) Holland, G.P., "Combining Solution and Solid-state NMR to Probe Spider Silk Assembly" Southern California Users of Magnets Meeting, Sanford Burnham Prebsy Medical Discovery Institute, La Jolla, CA (2015).

2) Davidowski, S.K., Amin, S.A., Cherry, B.R., Holland, G.P., Yarger, J.L., "Proton Detected HETCOR for Disordered Solids" Experimental NMR Conference, Pacific Grove, CA (2015).

3) Shi, X, Holland, G.P., Yarger, J.L., "Molecular Dynamics of Spider Silk Protein Investigated by Solid-state Deuterium Nuclear Magnetic Resonance" 26th International Council on Magnetic Resonance in Biological Systems, Dallas, TX (2014).

4) Guo, C., Holland, G.P., Yarger, J.L., "Silk-inorganic Nanocomposite Materials" American Chemical Society 247th National Meeting, Dallas, TX (2014).

5) Xu, D, Yarger, J.L., Holland, G.P., "Are Spider Silk Proteins a New Class of Intrinsically Disordered Proteins?" Biophysical Society 58th Annual Meeting, San Francisco, CA (2014).

6) Holland, G.P., "Spider's Silk: From Protein-rich Gland Fluids to Diverse Biopolymer Fibers" DOD-AFOSR, Natural Materials, Systems and Extremophiles, Program Review, Fort Walton Beach, FL (2014).

7) Holland, G.P., "Spider Silk Structure, Dynamics and Assembly: New Insights from NMR" Departmental Seminar – Chemistry and Biochemistry, San Diego State University, San Diego, CA (2014).

8) Holland, G.P., "Reverse Engineering Spider's Silk: Using NMR to Determine Structure, Dynamics and Assembly" Departmental Seminar – Chemistry, Colorado School of Mines, Golden, CO (2014).

9) Holland, G.P., "Spider's Silk: From Protein-rich Gland Fluids to Diverse Biopolymer Fibers" Functional Polymeric Materials Conference, Cancun, Mexico (2014).

10) Addison, J.B., Weber, W.S., Mou, Q., Holland, G.P., Yarger, J.L., "Structural Characterization of Caddisfly Silk with Solid-state NMR and X-ray Diffraction" Biophysical Society 58th Annual Meeting, San Francisco, CA (2014).

11) Holland, G.P. "Spider's Silk: From Protein-rich Gland Fluids to Diverse Biopolymer Fibers" DOD-AFOSR, Natural Materials, Systems and Extremophiles, Program Review, Fort Walton Beach, FL (2013).

b. Consultive and Advisory Functions: None
c. Technology Assists, Transitions, and Transfers: None

8. New discoveries, inventions, or patent disclosures: None

9. Honors/Awards: None

1.

1. Report Type

Final Report

Primary Contact E-mail

Contact email if there is a problem with the report.

gholland@mail.sdsu.edu

Primary Contact Phone Number

Contact phone number if there is a problem with the report

619-594-1596

Organization / Institution name

Arizona State University

Grant/Contract Title

The full title of the funded effort.

Spider's Silk: From Protein-Rich Gland Fluids to Diverse Biopolymer Fibers

Grant/Contract Number

AFOSR assigned control number. It must begin with "FA9550" or "F49620" or "FA2386".

FA9550-14-1-0014

Principal Investigator Name

The full name of the principal investigator on the grant or contract.

Gregory P. Holland

Program Manager

The AFOSR Program Manager currently assigned to the award

Hugh DeLong

Reporting Period Start Date

12/01/2015

Reporting Period End Date

11/30/2015

Abstract

The primary objective of this research is to elucidate the interactions, mechanisms and biochemistry of the spider silk producing process at the molecular level. Our primary focus is to characterize the protein-rich fluid in the various spider silk producing glands. We have been using a battery of magnetic resonance methods including solution and solid-state nuclear magnetic resonance (NMR) and micro imaging (MRI) in combination with wide angle and small angle X-ray diffraction (WAXD and SAXD) techniques at Argonne National Laboratory (ANL) to probe silk protein structure and dynamics prior to and following fiber formation. We have established a number of methods for isotopically (2H/13C/15N) enriching the silk proteins during the course of our AFOSR funding that have allowed us to investigate the structure, dynamics, and organization of spider silk protein within the silk gland and in the final spun fiber with a range of magnetic resonance methods. We successfully developed magnetic resonance imaging (MRI) techniques with localized spectroscopy to probe the silk glands of spiders and map protein structure through out the silk gland. We continue to develop MRI as an in vivo tool for interrogating silk protein structure and dynamics within the different silk glands and have been moving in a direction where we are imaging and conducting localized 1H NMR spectroscopy on silkworms where the internal spinning system is considerably larger compared to spiders. This work has greatly increased our understanding of spider silk and the silk producing process. This information will be useful for scientists trying to reproduce this

biologically inspired process in the laboratory.

Distribution Statement

This is block 12 on the SF298 form.

Distribution F - Further Dissemination Only as directed by the Controlling Office

Explanation for Distribution Statement

If this is not approved for public release, please provide a short explanation. E.g., contains proprietary information.

Report contains some published and some unpublished work.

SF298 Form

Please attach your SF298 form. A blank SF298 can be found here. Please do not password protect or secure the PDF
The maximum file size for an SF298 is 50MB.

SF298.pdf

Upload the Report Document. File must be a PDF. Please do not password protect or secure the PDF . The maximum file size for the Report Document is 50MB.

GPHolland_Final_Report_AFOSR_2015.pdf

Upload a Report Document, if any. The maximum file size for the Report Document is 50MB.

Archival Publications (published) during reporting period:

Changes in research objectives (if any):

Change in AFOSR Program Manager, if any:

Extensions granted or milestones slipped, if any:

AFOSR LRIR Number

LRIR Title

Reporting Period

Laboratory Task Manager

Program Officer

Research Objectives

Technical Summary

Funding Summary by Cost Category (by FY, $K)

	Starting FY	FY+1	FY+2
Salary			
Equipment/Facilities			
Supplies			
Total			

Report Document

Report Document - Text Analysis

Report Document - Text Analysis

Appendix Documents

2. Thank You

E-mail user

Dec 15, 2015 16:47:29 Success: Email Sent to: gholland@mail.sdsu.edu